

## **In-situ measurement of ground impedances**

Von der Fakultät für Mathematik und Naturwissenschaften der Carl von Ossietzky  
Universität Oldenburg zur Erlangung des Grades und Titels eines  
Doktors der Naturwissenschaften (Dr. rer. nat.)  
angenommene Dissertation

von

Herrn Roland Kruse,  
geboren am 23.12.1975 in Oldenburg (Oldb)

Gutachter: Prof. Dr. Volker Mellert  
Zweitgutachter: Prof. Dr. Jesko Verhey

Tag der Disputation: 27. November 2008

## Table of contents

I. Table of figures.....	5
II. Abstract.....	7
III. Zusammenfassung.....	8
IV. Introduction.....	9
Outdoor sound propagation .....	9
V. Definitions.....	11
VI. Surface impedance measurement methods.....	13
Laboratory methods.....	13
Kundt's tube.....	13
Impedance tube.....	13
Reverberation chamber.....	14
In-situ methods.....	14
Direct methods .....	14
Standing wave method.....	14
Tamura method.....	15
Pulse- echo methods :	
Separation of direct and reflected pulse in the time domain.....	15
Indirect methods (Sound field matching).....	16
Sound pressure based.....	16
Level difference versus excess attenuation.....	21
Field impedance based .....	22
Summary: In-situ impedance measurement.....	24
VII. Sound field models.....	25
Sound field above an infinite locally reacting impedance plane.....	25
The Nobile&Hayek solution .....	25
Effect of the approximations.....	29
Local and extended reaction .....	31
Effective impedance.....	32
Semi-infinite media.....	32
Layered media.....	32
Rough surfaces.....	33
VIII. External influences.....	35
Turbulence.....	35
Unwanted reflections.....	38
IX. Absorber models.....	39
Delany- Bazley / Miki (One parameter).....	39
Exponential changing porosity (Two / three parameters).....	40
Micro-structural model (Three / four parameters).....	40
Overview of absorber parameters of grounds.....	42
X. Effect of ground condition.....	46
Water saturation.....	46
XI. Published results.....	47
Acta Acustica: Application of the two-microphone method for in-situ ground impedance measurements (P1).....	47
Applied Acoustics: Effect and minimization of errors in in-situ ground impedance measurements (P2).....	47
Acta Acustica: Reducing the influence of microphone errors on in- situ ground impedance measurements (P3).....	47
JASA: Measuring the free field acoustic impedance and absorption coefficient of sound absorbing materials with a combined particle velocity - pressure sensor (P4).....	47
XII. Summary and conclusion.....	49
The standard ANSI S1.18 procedure.....	49
Analysis of the problem.....	49

Optimised geometry.....	50
Reducing the influence of microphone errors.....	50
Additional sources of errors: The sound source.....	50
Experimental verification, combination of optimised geometry and switched microphone technique .....	51
Microflown based measurements .....	53
XIII.Outlook.....	55
A global optimisation including external influences.....	55
The measurement equipment.....	55
Optimising microflown based sound field matching.....	55
General concerns .....	56
XIV.References.....	57
XV.Table of abbreviations.....	61
XVI.Publications.....	65

## I. Table of figures

Figure 1: Separation of direct and reflected pulse by windowing.....	15
Figure 2: Set-up for the transfer function method to determine the surface impedance.....	17
Figure 3: Measuring the surface impedance of a lawn with the transfer function method with two vertically separated microphones. ....	17
Figure 4: Level difference versus effective flow resistivity (from 10 to 10000 krayl/m) of the Delany-Bazley absorber model. Geometry A from ANSI S1.18.....	18
Figure 5: Phase gradient versus height above an impedance plane for a source height of 7 meters, a frequency of 100 Hz and a normalised surface impedance of $10 + 15i$ and $2 + 3i$ .....	20
Figure 6: Excess attenuation versus effective flow resistivity (from 10 to 10,000 krayl/m) of the Delany-Bazley absorber model. Geometry A from ANSI S1.18 (upper microphone). ....	21
Figure 7: Reflection coefficient measurement with a microflown orientated in a way that it only detects the velocity originating from the mirror source.....	24
Figure 8: Sound field above a locally reacting impedance plane at 100 Hz. Sound pressure in dB re. free field @ 1 m. Surface impedance = $(10 + 15i)$ . Source height is 1 m.....	27
Figure 9: Sound field above a locally reacting impedance plane at 100 Hz. Vertical velocity in dB re. free field @ 1 m. Surface impedance = $(10 + 15i)$ . Source height is 1 m.....	27
Figure 10: Sound field above a locally reacting impedance plane at 1 kHz. Sound pressure in dB re. free field @ 1 m. Surface impedance = $(2 + 3i)$ . Source height is 1 m.....	28
Figure 11: Sound field above a locally reacting impedance plane at 1 kHz. Vertical velocity in dB re. free field @ 1 m. Surface impedance = $(2 + 3i)$ . Source height is 1 m.....	28
Figure 12: Comparison of plane wave ( $R_p$ ) and spherical reflection coefficients ( $Q_1 / Q_5$ ) for geometry A from ANSI S1.18 (upper microphone) and a locally reacting ground with a flow resistivity of 100 krayl/m (Delany-Bazley model).....	30
Figure 13: Comparison of the spherical wave reflection coefficient $Q$ using the exact numerical distance ( ) (eq.29) and it's approximation (---) (eq.31). Geometry A (upper microphone) and DB model with three flow resistivities.....	31
Figure 14: Difference in the effective surface impedance $Z$ between local and extended reaction (semi-infinite or 10cm layer with hard backing) for a material with a flow resistivity of 10 krayl/m. Geometry A ( $\theta = 24^\circ$ ).....	33
Figure 15: Difference in the effective surface impedance $Z$ between local and extended reaction (semi-infinite or 10cm layer with hard backing) for a material with a flow resistivity of 100 krayl/m. Geometry A ( $\theta = 24^\circ$ ).....	33
Figure 16: Comparison of the effective surface impedance of a smooth and a rough surface. DB model, effective flow resistivity 100 krayl/m. Mean roughness height is 1 cm. ....	34
Figure 17: Effect of strong turbulence on the excess attenuation for three source and receiver heights $h$ and a source-receiver distance of 1.75m. Impedance from Delany-Bazely model with an effective flow resistivity of 100 krayl/m. ( ) without, (---) with turbulence. ....	36
Figure 18: Effect of strong and low turbulence on the excess attenuation. Difference between EA with and without turbulence. $R = 3$ m, $h_s = 0.5$ m, $h_{rl} = 0.05$ m ( ) and $h_{ru} = 0.95$ m (---). Effective flow resistivity = 100 krayl/m.....	37
Figure 19: Variability of the level difference spectrum: mean level difference $\pm$ standard deviation. Geometry A. Some background noise and wind speeds of 3 -4 (5) m/s. Sand area.....	37
Figure 20: Comparison of the characteristic impedance $Z_c$ predicted by the four parameter model (H4A), the three parameter (H3A), the one parameter (H1A) approximation, the Miki and the Delany-Bazley model. $\sigma = 100$ krayl/m, $\Omega = 0.4$ , $n = 1$ and $sp = 0.2$ .....	42
Figure 21: Ground impedance of a compacted, dry lawn. Comparison of results obtained with small loudspeaker (10 cm) and large woofer (25 cm). Geometry: $h_s = 0.8$ m, $h_{ru} = 1$ m, $h_{rl} = 5$ cm and $R = 5$ m. ....	51
Figure 22: Impedance of sand measured with geometry A from ANSI S1.18. Switched microphones technique: microphones in "normal" position (Normal), microphones' positions switched (Inverse) and corrected/ mean transfer function from both measurements (Mean). ....	52
Figure 23: Impedance of sand measured with the optimised geometry from publication P2. $h_s = 0.5$ m, $h_{ru} = 0.95$ m, $h_{rl} = 5$ cm and $R = 3$ m. Switched microphones technique. ....	52
Figure 24: Impedance of sand measured with a large optimised geometry. $h_s = 0.8$ m, $h_{ru} = 1.3$ m, $h_{rl} = 5$ cm and $R = 5$ m. Switched microphones technique.....	53



## II. Abstract

The sound propagation outdoors is subject to manifold physical influences of the propagation path. Independent of the method used for the prediction (empirical or analytical model), precise input data is needed to calculate the propagation loss. For distances less than 100 meters, for which meteorological effects play a minor role, the properties of the ground – typically given by the surface impedance – are most important.

For determining the ground impedance, a number of procedures are available; to obtain representative results, in-situ procedures are preferable as the (small) samples used for laboratory methods cannot take into account the inhomogeneity and layering of the ground.

This work investigates which of these procedures, with respect to their reliability and ease of use, are suited for determining ground impedances and which factors influence the measurement accuracy. For this purpose, an overview of current laboratory and in-situ techniques for impedance measurements is given at first. A presentation of the sound field model employed by many of these methods, especially those from which a good performance can be expected in the lower frequency range (below 500 Hz), follows. For the subsequent evaluation of ground impedance measurements, selected models for the prediction of the impedance of porous absorbers are presented and a tabular overview of absorber parameters of a large number of grounds is given. Furthermore, several “external” factors which can affect in-situ impedance measurements are discussed.

In the main part of this work, the adequacy of a partially standardised (ANSI S1.18) method, the two-microphone or transfer function method, is tested for a number of grounds. It turns out that the method already achieves reproducible and credible results, but only for frequencies above approx. 400 Hz and not for acoustically hard grounds.

In order to better understand this behaviour, a numerical simulation is used to forecast the effect of unavoidable measurement uncertainties on the predicted impedance. Even small errors in the transfer function in the range of accuracy of high quality measurement systems cause considerable errors in the ground impedance. In addition, inaccuracies in the microphones' positions can't be neglected. To increase the reliability of the two-microphone technique, two improvements are developed. On the one hand, estimates of the surface impedance and the measurement uncertainties are used to find geometries which show an average error in the predicted impedance as small as possible, in a given frequency range. On the other hand, differences in the microphones are a source of errors in the transfer function. To compensate these errors, measurements with the microphones in normal and switched positions – analogue to the course of action for impedance tube measurements (ISO 10534-2) – are suggested.

Both optimisations, the selected geometries and switching of the microphones, are verified experimentally, whereupon the combination of both measures is also kept in mind. The result is a substantial improvement of the accuracy below 500 Hz, so that reliable measurements above 100 Hz are made possible. In this context, it was additionally discovered that the type of sound source can have a significant influence on the low frequency performance so that, contrary to the recommendations of ANSI S1.18, the application of large loudspeakers has to be advised. Over and above the investigation of the two-microphone method, the alternative usage of a microflown to directly determine the field impedance has been investigated under laboratory conditions. It turns out that a performance comparable to the two-microphone technique can be achieved, but no advantage of using a microflown could be found in light of the practical difficulties in using this sensor.

The finish of this work is formed by an outlook which points out the numerous unanswered and newly arisen questions in connection with in-situ impedance measurements. Even though the proposed measurement procedure is currently the method of choice for determining ground impedances, it becomes obvious that future improvements are still possible.

### III. Zusammenfassung

Die Schallausbreitung im Freien unterliegt vielfältigen physikalischen Einflüssen des Ausbreitungspfades. Unabhängig von der zur Vorhersage verwendeten Methode (empirisches oder analytisches Modell) sind zur Berechnung der Ausbreitungsdämpfung präzise Eingangsdaten erforderlich. Im Bereich von Entfernungen unter 100 Metern, in dem meteorologische Einflüsse nur eine geringe Rolle spielen, sind besonders die Eigenschaften des Bodens – üblicherweise gegeben durch die Oberflächenimpedanz - von großer Bedeutung.

Zur Bestimmung der Bodenimpedanz stehen eine Reihe von Verfahren zur Verfügung; um repräsentative Ergebnisse zu erhalten bieten sich in-situ Verfahren an, da die für Laborverfahren verwendeten (kleinen) Proben die Inhomogenität und Schichtung des Bodens nicht berücksichtigen können.

Die vorliegende Arbeit untersucht, welche dieser Verfahren unter dem Gesichtspunkt der Zuverlässigkeit und Anwendungsfreundlichkeit für die Ermittlung der Bodenimpedanz geeignet sind und welche Größen Einfluss auf die Messgenauigkeit nehmen. Zu diesem Zweck wird zunächst ein Überblick über die existierenden Labor- und in-situ Verfahren der Impedanzmessung gegeben. Es schließt sich eine Darstellung des Schallfeldmodells an, dass von mehreren dieser Verfahren verwendet wird, insbesondere denen, die auch gute Ergebnisse im Bereich tieferer Frequenzen (unter 500 Hz) erwarten lassen. Zur Bewertung späterer Messergebnisse der Bodenimpedanz werden einzelne verbreitete Modelle zur Vorhersage der Impedanz von porösen Absorbern präsentiert, und es wird ein tabellarischer Überblick über die Absorberparameter einer größeren Anzahl von Böden gegeben. Des Weiteren werden verschiedene „äußere“ Faktoren diskutiert, die grundsätzlich Einfluss auf in-situ Impedanzmessverfahren haben können.

Im Hauptteil der Arbeit wird zuerst die Eignung eines teilweise standardisierten (ANSI S1.18) Verfahrens, des Zweimikrofon oder Transferfunktionsverfahrens, für verschiedene Böden getestet. Es zeigt sich, dass dieses Verfahren bereits reproduzierbare und glaubwürdige Ergebnisse erzielt, jedoch nur im Bereich über ca. 400 Hz und nicht für akustisch harte Böden.

Um dieses Verhalten besser zu verstehen wird eine numerische Simulation verwendet, um den Effekt unvermeidbarer Messunsicherheiten auf die vorhergesagte Impedanz zu ermitteln. Bereits geringe Fehler in der Transferfunktion im Bereich der Genauigkeit hochwertiger Messsysteme bewirken erhebliche Fehler in der Bodenimpedanz. Auch Ungenauigkeiten in der Mikrofonpositionierung sind nicht zu vernachlässigen.

Um die Zuverlässigkeit der Zweimikrofonmethode zu erhöhen werden zwei Verbesserungen entwickelt. Zum einen werden unter Zuhilfenahme von Schätzwerten der Bodenimpedanz und der Messunsicherheiten Geometrien bestimmt, die in einem gegebenen Frequenzbereich einen möglichst geringeren mittleren Fehler in der vorhergesagten Impedanz aufweisen. Andererseits stellen Unterschiede in den verwendeten Mikrofonen einen Grund für Fehler in der Transferfunktion dar. Um diesen Fehler zu kompensieren wird die Messung mit den Mikrofonen in normaler und vertauschter Position – analog der Vorgehensweise bei Impedanzrohrmessungen (ISO 10534-2) – empfohlen. Beide Optimierungen, die ausgewählten Geometrien und die Vertauschung der Mikrofone, werden experimentell überprüft, wobei auch die Kombination dieser Maßnahmen berücksichtigt wird. Es ergibt sich eine wesentliche Verbesserung der Messgenauigkeit unterhalb 500 Hz, so dass zuverlässige Messungen ab 100 Hz ermöglicht werden. In diesem Zusammenhang wurde weiterhin festgestellt, dass auch die Art der Schallquelle einen bedeutenden Einfluss auf die Genauigkeit bei tieferen Frequenzen haben kann, und es muss entgegen den Empfehlungen der ANSI S1.18 der Einsatz großer Lautsprecher angeraten werden.

Zusätzlich zur Untersuchung der Zweimikrofonmethode wurde alternativ die Verwendung eines Microflowns zur Direktmessung der Feldimpedanz (unter Laborbedingungen) untersucht. Es ergab sich eine dem Zweimikrofonverfahren vergleichbare Leitungsfähigkeit, jedoch kann auch aufgrund praktischer Probleme im Zusammenhang mit dem Gebrauch von Microflowns derzeit kein Vorteil in der Nutzung dieses Sensors erkannt werden.

Den Abschluss der Arbeit bildet ein Ausblick, der auf die zahlreichen offen gebliebenen und neuen Fragen in Zusammenhang mit der in-situ Messung der Impedanz aufmerksam macht. Wenngleich das vorgeschlagene Messverfahren derzeit die Methode der Wahl zur Bestimmung der Bodenimpedanz ist wird erkennbar, dass noch weitere Verbesserungen möglich sind.



## IV. Introduction

### Outdoor sound propagation

The propagation of sound outdoors is a topic not only of scientific but also of economic concern. There are a number of man-made source of sound or, more precisely, noise in the sense of unwanted sound: means of transport (cars, railways, aircraft), construction sites, factories (heavy machinery) or wind turbines. The question will often be: what sound levels have to be expected at a specific location, a place where people reside, recreate or work? Alternatively, what can be done to reduce the existing immission levels?

The sound level will depend on two factors: the characteristics of the source (sound power, spectrum, directivity) and the characteristics of the propagation path. Sound is attenuated when it propagates outdoors, the total attenuation being the combination of several effects. First and foremost, spreading of the wave fronts leads to a declining sound pressure, the rate depending on the type of source (point source, line source). Atmospheric absorption is the result of shear viscosity, heat conduction and molecular relaxation losses. Geometric obstacles, either natural or artificial, impede the sound propagation. The atmosphere traversed by the sound wave is generally not homogeneous: sound speed gradients from wind and thermal layering lead to refraction, turbulence to diffusion. Finally, the sound interacts with the ground over which it passes.

The relative importance of these factors depends on the distance. For distances in the order of one kilometre or above, the atmospheric conditions will regularly have the highest influence. On the other hand, for distances of a few tens to one hundred metres, propagation is severely influenced by ground effects. In addition, the total attenuation depends on the frequency, with low frequency sound experiencing less attenuation.

There are a number of schemes for the prediction of the total sound attenuation which will occur in a specific situation. The most popular ones are empirical (or engineering) models due to their ease of use (no complicated math) and the fact that they're partly standardised. They model the total attenuation as the sum of individual factors, like the ones presented above, and provide either tables or simple equations to determine these factors. Examples are ISO 9613-2 [1] and the HARMONOISE/ IMAGINE model [2].

A more sophisticated approach is to model the actual physical process of wave propagation in the atmosphere, the use of an analytic model. With the exact solution of the wave equation being too computational heavy, one has to revert to approximations in the form of parabolic equation (PE) or fast field program (FFP). For an overview of these methods, Salomon's book on atmospheric acoustics may be recommended [3].

No matter what model is used, the predictions will only be as good as the input data. In case of analytical models this means a sound speed profile (combining the effects of wind and temperature) and an adequate description of the acoustical properties of the ground. For the ground, the procedures will rely either on an absorber model to determine the acoustical (and sometimes even the mechanical) properties, or on measured surface impedances.

This investigation deals with the question of how to obtain dependable impedance estimates with special regard to the frequency range below 500 Hz.

There are a number of techniques for measuring the surface impedance or reflection coefficient of materials, which can be classified into laboratory and in-situ techniques. Some of these have become standardised, some are new and little is known about their performance. The first task of this work will be to give an overview of methods for impedance measurements in order to identify those who promise to deliver reliable results in the frequency range below 500 Hz during outdoor use.

Some of the methods, especially the ones that will at least theoretically be functional for lower frequencies, make use of a sound field model to deduce the surface impedance. The model which is used throughout this work will be presented and the inherent approximations and assumptions will be discussed.

The measurement procedures and sound field model allow for the determination of the surface impedance, but for evaluation of the results one needs to have an idea of how a typical ground impedance, for a number of different grounds and ground structures, looks like. A short overview of absorber models will therefore be given together with a compilation of absorber parameters for a number of grounds.

By use of all these informations, the suitability of two selected measurement procedures, the two-microphone transfer function method and the use of a field intensity probe, for the envisaged purpose is investigated in the main part of this work.

Subsequently, two improvements for the two-microphone methods will be suggested which lead to a significantly improved performance of this method in the frequency range below 400 Hz. This main part of the work consists of four peer reviewed papers published, or accepted for publication, in relevant acoustical journals.

The results will then be summarised to gain an overall picture of the performance of the improved transfer function method. For that purpose, some additional results will have to be presented which were not previously published.

Not all questions could be answered in this text, and neither will the suggested method be perfect. In the outlook section, hints will be given concerning what can be done to further refine the measurement technique and what general questions have to be answered to obtain representative ground impedance predictions.

This thesis has been influenced by the current work on the revision of the standard ANSI S1.18 for the deduction of ground impedances, and some of the results and recommended refinements have already been included in the latest draft standard [4].

I would hereby like to thank the members of ANSI S1 workgroup 20 for their support and helpful suggestions.

## V. Definitions

The following section will give an overview of basic terms used in this work. The use of these terms in the literature is sometimes non-uniform and special attention should be placed to the boundary conditions which apply to these definitions.

### The velocity potential

A sound field can be characterized by any of the state variables of the fluid: Pressure, particle velocity, density or temperature. In practise, one will choose the variable which can most easily and accurately be measured, the sound pressure. However, for a theoretical description of a sound field it is often more useful to benefit from the fact that a sound field is an irrotational vector field and can thereby be given by a scalar field, the velocity potential  $\Phi$ .

Sound pressure  $p$  and particle velocity  $u$  are then given by eq.1 and 2,  $\omega$  being the angular frequency and  $\rho_0$  the equilibrium density of the fluid. An  $\exp(-i\omega t)$  time dependency is assumed.

$$p = \rho_0 \cdot \frac{\partial \Phi}{\partial t} = -i \cdot \omega \cdot \rho_0 \cdot \Phi \quad (1)$$

$$u = -\nabla \Phi \quad (2)$$

With the velocity potential being proportional to the sound pressure for any given frequency, ratios of velocity potentials are equal to ratios of sound pressures.

### Impedance and admittance

The field impedance  $Z_i$  is the ratio of the complex amplitudes of the sound pressure and the particle velocity  $u_i$  in a given direction  $i$  at any location in the sound field (equation 3).

$$Z_i = \frac{P}{u_i} \quad (3)$$

A special case of the field impedance is the characteristic impedance  $Z_c$  which is the field impedance of a plane wave in the direction of the wave propagation. It is equal to the product of density and sound velocity in the fluid. For air, it is equal to  $Z_0 = \rho_0 c_0 = 413.3$  MKS rayl at 20°C. The characteristic impedance is a material constant and, together with the wave number, fully describes the acoustical properties of a (homogeneous and isotropic) fluid.

The surface impedance  $Z$ , on the other hand, is the field impedance for the surface normal component of the velocity directly on a surface. It is important to note that it is generally understood that the surface impedance is given for an incident plane wave and that the field impedance at a surface can be different from this surface impedance in other cases. The surface impedance is not a material constant but describes the properties a surface, which can even be an imaginary plane in the sound field. As will later be discussed, it can depend on the angle of incidence of the sound wave.

An admittance  $\beta$  is defined as the inverse of the respective impedance.

### Reflection and absorption coefficient

For many applications – especially in room acoustics – it is desirable not only to know the impedance of a surface but also the ratio of the sound pressures of reflected to incident wave (reflection coefficient) and the amount of energy dissipated by the material (absorption coefficient). For a plane wave with an angle of incident  $\theta$  relative to the surface, the reflection coefficient  $R_p$  follows from simple geometric considerations (eq.4).

$$R_p = \frac{Z \sin(\theta) - 1}{Z \sin(\theta) + 1} = \frac{\sin \theta - \beta}{\sin \theta + \beta} \quad (4)$$

Equation 4, though widely used, is a simplification only valid if the wave number  $k_m$  of the material is high or for (near) normal incidence. Otherwise, equation 5 has to be used,  $k'$  being the normalised wave number (equal to the index of refraction) in the material (eq.6).

$$R_p = \frac{Z \sin(\theta) - \chi}{Z \sin(\theta) + \chi} \text{ with } \chi = \sqrt{1 - \frac{1}{k'^2} \cos^2 \theta} \quad (5)$$

and

$$k' = \frac{k_m}{k} = \frac{c_0}{c_m} \quad (6)$$

The intensity of a wave being proportional to the sound pressure squared, the ratio  $\alpha$  of energy not reflected by the surface, the absorption coefficient, is given by eq.7.

$$\alpha = 1 - |R_p|^2 \quad (7)$$

Only if the material does not show sound transmission, either because it is semi-infinite or hard backed,  $\alpha$  is equal to the amount of sound energy dissipated by the material.

### Excess attenuation

For the description of sound fields, it is convenient not to use absolute values of the sound pressure or velocity because these will depend on the source strength. It is better to compare measured values with a "reference" situation. A common choice is the free field situation where no reflections from a surface are present. The excess attenuation EA is the ratio of the sound pressure  $p$  by the free field sound pressure  $p_{\text{free field}}$  keeping the distance between source and receiver and the source strength constant (eq.8).

$$EA = -20 \lg \frac{p}{p_{\text{free field}}} \quad (8)$$

If expressed in decibels, a positive value will imply that the sound pressure is lower than the sound pressure in a free field.

## VI. Surface impedance measurement methods

### Laboratory methods

Laboratory methods for the determination of absorption or reflection coefficients are all methods which either require that samples be cut from the material under investigation or which use an experimental set-up or facilities which can't regularly be utilised outside a laboratory environment.

#### Kundt's tube

The oldest and longest used procedure for measuring reflection coefficients of material samples is the Kundt's or standing wave tube. This technique is standardised in ISO 10534-1 [5]. In a tube with a diameter  $d$  small enough to only support wave propagation in axial direction ( $d < 0.58\lambda$  for a circular tube), a loudspeaker is placed at one end and the other opening at distance  $l$  is terminated by a hard backing. These boundary conditions allow for a standing wave to develop if

$$l = (2a - 1) \frac{\lambda}{4}, \quad a \in \mathbb{N} \quad (9)$$

The standing wave ratio  $n$  measured with a moveable probe microphone depends on the reflection coefficient  $R_p$ .

$$n = \frac{p_{min}}{p_{max}} = \frac{1 - |R_p|}{1 + |R_p|} \quad (10)$$

To calculate the surface impedance, the phase of the reflection coefficient has to be measured by determining the position of the first pressure minimum relative to the sample surface. The Kundt's tube is a robust method for surface impedance measurements requiring only simple equipment. Its main disadvantages are the high time need and that only a limited number of frequencies can be used. Highly absorbing samples make the identification of the standing wave ratio and position of first minimum difficult. On the other hand, it is well suited for materials with low absorption though one may need to account for the propagation loss in the tube due to viscous friction at the tube walls if a high accuracy is required.

#### Impedance tube

The two microphone impedance tube is the state of the art device for measuring the complex reflection coefficient of samples in the laboratory. It is standardised in ISO 10534-2 [6]. The set-up is comparable to the Kundt's tube built-up, but two microphones at fixed positions are used. The microphones receive both the incident and reflected wave; the transfer function  $H_{12}$  between the two microphones' signals is a function (eq. 11) of the geometry and the reflection coefficient,  $x_1$  and  $x_2$  being the distance between surface and microphone 1 resp. 2 and FT the Fourier transform.

$$R_p = \frac{H_{12} e^{ikx_2} - e^{ikx_1}}{H_{12} e^{-ikx_2} - e^{-ikx_1}} \quad \text{with} \quad H_{12} = \frac{FT(p_1)}{FT(p_2)} \quad (11)$$

This method allows for a rapid determination of the plane wave reflection coefficient and thereby the surface impedance in a wide frequency range. Its accuracy depends mainly on the accuracy of the transfer function. At low frequencies, the distance between the microphones becomes small compared to the wavelength making the phase angle measurements inaccurate (it is therefore recommended at the distance be at least 5% of  $\lambda$ ). It can be shown that the maximum accuracy is obtained if the microphone's separation is equal to  $\frac{1}{4} \lambda$  with accuracy severely decreasing if nearing  $\frac{1}{2} \lambda$  [7]. If the samples exhibits low absorption, a standing wave can develop at the respective frequencies with one of the microphones being located at or near a pressure minimum. It has therefore be recommended to use more than two microphones or allow for the positioning of the microphones at different locations of the tube [8].

## Reverberation chamber

Measurement of the absorption coefficient in a reverberant chamber is a procedure in accordance with ISO 354 [9]. In the diffuse field of such a chamber, the reverberation time  $T_{60}$  for a 60dB decrease in sound pressure level depends on the total "amount" of absorption. A commonly used, though simplified, relationship is the Sabine's equation [10]:

$$T_{60} = \frac{V}{\alpha \cdot S} \quad (12)$$

with  $V$  being the volume of the chamber and  $S$  the exposed surface area of the material sample. The absorption coefficient gained is the absorption coefficient for random incidence. Reverberation chamber measurements do not provide any information about the complex reflection coefficient or the surface impedance of the sample. For low frequencies, large rooms are needed to ensure a sufficient modal density, otherwise the sound field may not be considered diffuse. Results will also depend on the sample size and distribution in the chamber as well as the characteristics of the respective reverberation chamber [11]. A clear advantage is the possibility to investigate large samples or constructions.

The presented laboratory methods, though capable of providing highly accurate results, have a number of drawbacks. The material samples used are generally small compared to the actual absorbing structure to be characterised, be it a ground outdoors or an absorber installed in a room. Whenever the structure is inhomogeneous, layered, or has acoustical properties depending on its size, it is questionable whether the sample has the same properties. In addition, these methods are restricted to plane wave reflection and a fixed angle of incidence (normal or random incidence).

## In-situ methods

The following section will give an overview of procedures which have been suggested for measuring the reflection coefficient and/or impedance in-situ. Both, methods which have been used outdoors as well as methods which were used only in a laboratory environment but could be beneficial for ground impedance measurements, will be discussed.

### Direct methods

Direct methods for in-situ reflection measurements are all methods which do not rely on a model for the sound field above a surface (assume geometric reflection).

### Standing wave method

The use of the established Kundt's tube theory for ground impedance measurements has been suggested by [12]. An actual (acrylic) Kundt's tube is driven into the ground, but this procedure had limited success. While it worked under laboratory conditions for sand, it completely fail on turf. The tube changed the micro climate around the plants and condensation quickly occurred. Furthermore, driving the tube into the ground was cumbersome. An improved method is suggested using a horn loudspeaker placed 4 – 5 m above the ground. The sound pressure (standing wave envelope) between source and ground is measured with a microphone attached to a string which is guided by a pulley fixed to the loudspeaker. The surface impedance is deduced from the standing wave envelope keeping in mind the spreading and corresponding attenuation of the emitted spherical wave (in contrast to the plane wave assumption in the tube). Impedance and absorption data is presented between 200 and 1000 Hz. While the absorption data appears reasonable, the real part of the impedance is almost constant or even decreases with decreasing frequency, a behaviour that only thin layers with low flow resistivity above a hard backing show.

## Tamura method

The Tamura method [13,14] is based on the determination of the complex sound pressure distribution on two planes parallel to the surface under test. By spatial Fourier transform, the pressure distributions are decomposed into plane wave components. Reflection on the surface is thereby simplified to plane wave reflection, the incident and reflected component of the plane wave – and therefore the reflection coefficient – following from the sound pressure at the two locations above the surface. An advantage is the fact that the incident wave can be of any shape and that the reflection coefficient is obtained for arbitrary angles of incidence. In practise, a sound source showing rotational symmetry, especially a dipole source, is used so that it is sufficient to measure the sound pressure along two lines instead on two planes. Unfortunately, only measurement results gained in a semi-anechoic room for frequencies larger than 500 Hz are presented, but the results agree well with reflection coefficients predicted by assuming a hard backed layer with a characteristic impedance and propagation constant measured in an impedance tube.

Because by decomposing the wave into plane wave components the sound pressure distribution on the surface can be predicted, the Tamura method is directly related to near field holography.

## Pulse- echo methods :

### Separation of direct and reflected pulse in the time domain

Pulse- echo methods for reflection coefficient measurements are the most direct and easy to understand procedures for that purpose. They are the only in-situ methods which have been standardised in the European Union: ISO 13472-1 [15] describes their use for measuring the absorption coefficient of road surfaces. In CEN/TS 1793-5 ("Adrienne" method) [16] the use of this method is recommended for assessing the absorption of roadside noise barriers. The methods follow closely the definition of the reflection coefficient  $R_p$  as the ratio of the direct and reflected wave's sound pressure keeping in mind the (linear) decrease of sound pressure with distance (eq.13).  $d_{direct}$  and  $d_{reflected}$  denote the length of the direct and reflected path (or the associated delay).

$$R_p = \frac{d_{reflected}}{d_{direct}} \frac{FT(p_{reflected})}{FT(p_{direct})} \quad (13)$$

The impulse response of the surface is obtained using either the short pulse of a blank pistol [17] or, nowadays, by an MLS based measuring system [18,19]. Direct and reflected signal, included in the impulse response of the surface, are separated in the time domain. Two procedure are routinely used for that purpose: Windowing or subtraction of the direct signal.

Windowing relies on the two pulses being separated because of the delay between the direct and reflected signal (fig.1).

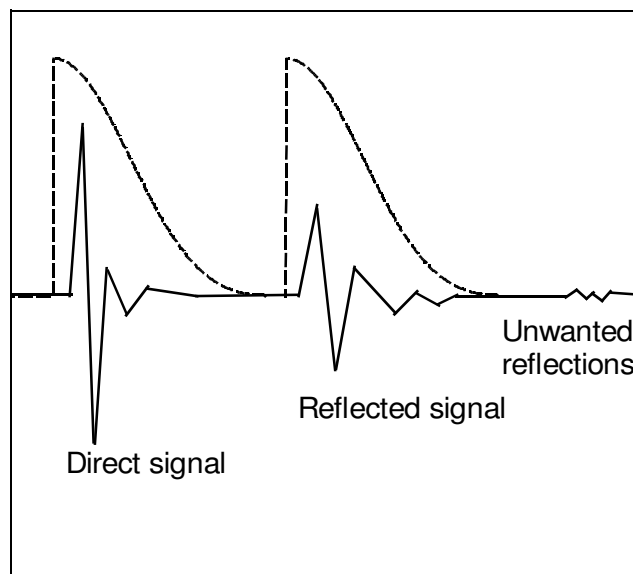


Figure 1: Separation of direct and reflected pulse by windowing.

The separation between the pulses will only be large enough if the path length difference is high and the length of the incident pulse is not too long. This requires a large set-up (one meter path length difference equals a delay of only approx. 3 ms) and to some extent the need to shorten the impulse response of the playback system (loudspeaker) by pre-equalisation of the MLS. The finite length of the window will deter the low frequency performance resulting in a lower frequency limit not less than the inverse of the window duration.

The subtraction technique [20] tries to overcome the limitation imposed by the short windows. In addition to the impulse response measurement near the surface, a reference measurement (direct pulse only) is done in a free field keeping the distance between source and microphone constant. The reflected pulse can now be isolated from the impulse response by subtraction of the reference measurement. While today it is simple to store and manipulate an impulse response with a personal computer, in former times researchers occasionally used a second microphone further away from the surface and analogue circuitry to subtract one signal from the other [17].

The pulse-echo method has caught increased attention during and after the Adrienne project [21] which led to the draft standard CEN/TS 1793. A number of shortcomings have been identified: The lowest reliable frequency for this method, though already decreased to 200 Hz by use of the subtraction technique instead of windowing, was still above the target limit of 100 Hz of the Adrienne project [21]. Additionally, the method did not perform well for noise barriers with a structured surface because of near field effects [22]. Other uncertainties identified [23] are the validity of the linear decrease of the sound pressure with distance or delay which will not be accurate for higher frequencies because of the finite size of the (piston) source and the rather small distance between source and surface. The sound source is also not a spherical source in the whole frequency range so that the direct and reflected pulse will, for other than normal incidence, not have the same free field sound pressure because they belong to different beam angles of the loudspeaker. Fortunately, a simple geometric correction – requiring the directivity pattern of the loudspeaker – is considered to be sufficient [24].

Summarising the properties of the pulse-echo method it can be said that this method is robust and easy enough for in-situ use [25] but should be limited to higher frequencies and near normal angles of incidence.

## Indirect methods (Sound field matching)

The in-situ methods presented so far assume that the reflection at the surface can be described by simple geometric considerations. The incident wave is considered to be plane just like the reflected wave. The only limitation taken into account is a linear decrease of sound pressure with distance. As will be shown in sect. 4, the sound field above an impedance plane is more complicated as long as frequency or distance between source and surface are not large. Or, in other words, as long as  $k \cdot R$  is not much larger than unity. The indirect methods thereby choose another approach: The measured characteristics of the sound field, e.g. the pressure transfer function between two locations, are compared with the predictions of a sound field model. The surface impedance is obtained by matching the prediction with the measurement.

### Sound pressure based

The sound field parameter most easily be measurable is the sound pressure and it is reasonable to measure the sound pressure at one or more locations to characterise the field above the surface.

#### Two microphones: Transfer function

A typical set-up for the two microphone or transfer function method is shown in fig.2 and 3. The sound pressure originating from the loudspeaker is measured simultaneously with two microphones at different locations. If rotational symmetry is assumed the transfer function between the two locations will totally characterise the sound field and depend only on the surface impedance and geometry. The depicted geometry is only an example. The sound source could as well be located above the microphones or the microphones being situated at different radial distances  $R$  from the source. However, as will later be shown, some geometries may be more favourable than others.



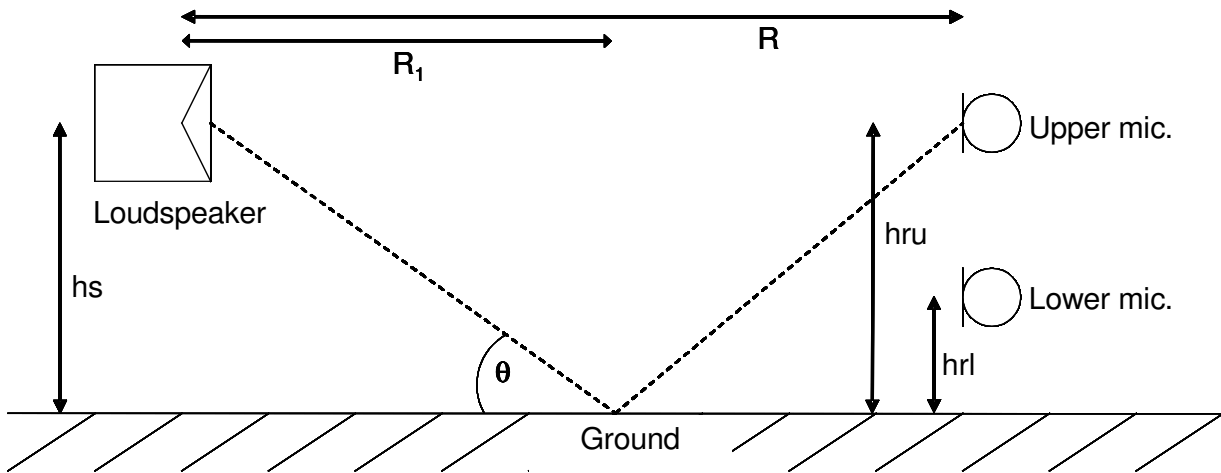


Figure 2: Set-up for the transfer function method to determine the surface impedance.



Figure 3: Measuring the surface impedance of a lawn with the transfer function method with two vertically separated microphones.

### Template method

The template method is standardised in ANSI S1.18 [26]. It allows for a very convenient determination of the surface impedance with only basic knowledge of acoustical measurements and without complicated mathematical routines. The user has to measure the level difference (magnitude only) between two microphone locations with one or more of three predefined source- receiver geometries (table 1). At least four measurements at different locations over the ground under test are averaged. The level difference spectrum is then compared, at first visually, with pre-calculated level difference spectra ("templates") for different combinations of absorber parameters, for two absorber models, as shown in fig.4. The template agreeing best with the data is selected by calculating 3<sup>rd</sup> octave averages and choosing the one that has the lowest sum-of-squares difference between measured values and values tabulated in the standard. The surface impedance follows from the absorber parameters. The template method is a robust and easy to use procedure but is restricted to the chosen absorber model(s).

Geometry	Source height	Distance source-receiver	Lower microphone height	Upper microphone height
A	32.5	175	23	46
B	20	100	5	20
C	40	100	5	40

Table 1: Source- receiver geometries for the two microphone / template method as suggested by ANSI S1.18. Data in centimetres.

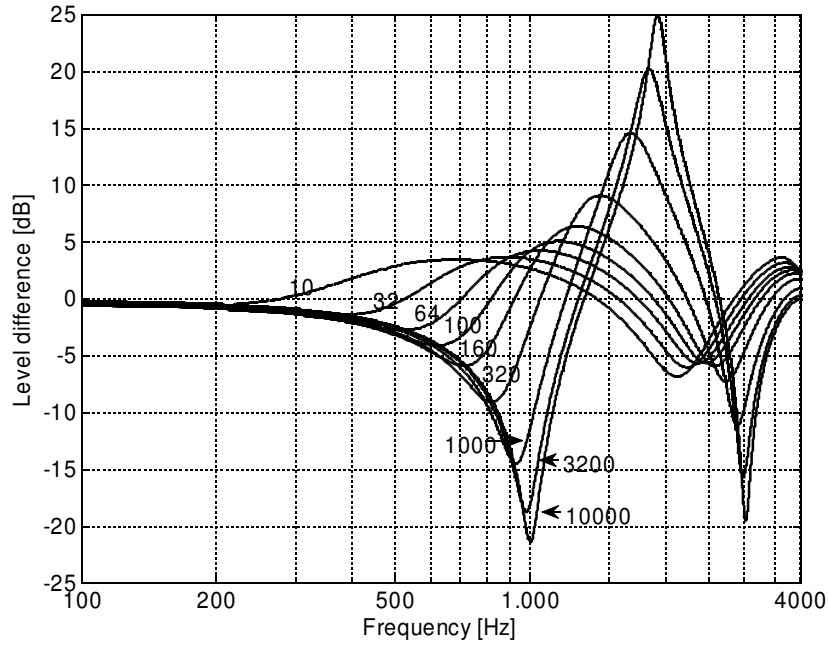


Figure 4: Level difference versus effective flow resistivity (from 10 to 10000 krayl/m) of the Delany-Bazley absorber model. Geometry A from ANSI S1.18.

### Direct deduction of ground impedance

A consistent advancement of the template method is the attempt to directly calculate the surface impedance from the (complex) level difference spectrum without restriction to an absorber model and hence a predefined course of the impedance. A number of different approaches have been chosen for that task. If plane wave or plane wave like reflection is assumed ("mirror source model") it is possible to derive the surface impedance  $Z$  analytically from the measured transfer function  $H_{12}$  (eq.14 for normal incidence spherical waves with plane wave like reflection [27]).

$$Z = \frac{(1+R_s)}{(1-R_s)} \left(1 - \frac{1}{ikh_s}\right) \text{ with } R_s = \left(\frac{e^{ikr_1}}{r_1} - H_{12} \frac{e^{ikr_2}}{r_2}\right) \left(H_{12} \frac{e^{ikr_2'}}{r_2'} - \frac{e^{ikr_1'}}{r_1'}\right)^{-1} \quad (14)$$

$(r_1, r_1')$  and  $(r_2, r_2')$  denote the length of the direct and reflected path for microphone 1 resp. 2 and  $h_s$  the height of the source above the surface.

This procedure has been used successfully for two microphones relatively close together for frequencies of 300 Hz and beyond [27,28] under laboratory conditions. It has also been applied under more realistic indoor and outdoor conditions using environmental noise (instead of a well defined sound source) [29] to obtain the absorption coefficient for random incidence above 200 Hz. Further improvements concerning the direct deduction of the surface impedance were hampered by the fact that it is often not possible to analytically solve the equations of more advanced sound field models for

the surface impedance. Thus, it is necessary to use numerical methods for the purpose of finding the surface impedance which minimises the difference between the observed level difference and the level difference predicted by the model. Progress in this area was predominantly delayed by the lack of adequate computing power. One of the first solutions was an iterative procedure [27] which calculates an estimate of the impedance assuming spherical waves but plane wave like reflection and then improves that estimate by using the “exact” sound field model to determine the level difference following from this. More recent suggestions are the use of a downhill simplex algorithm [30] and especially the Newton-Raphson root finding technique [31] which allows for an extremely fast calculation but requires the derivative of the velocity potential for the surface impedance/ admittance. While both aforementioned references use excess attenuation instead of level difference measurements, the methods can also be applied to the latter. Indeed, the direct deduction of surface impedance from level difference measurements using the Newton-Raphson procedure is currently under discussion to become an ANSI standard [4].

The proposed ANSI standard will suggest a combination of the template method and direct impedance deduction. The aim is to allow the user to compare both results in order to judge if they are reasonable or if additional measurements – with other geometries – are advisable. There has been quiet an extensive comparison of both methods [32] coming to the conclusion that the template method is in general preferable as being more robust, at least if only the magnitude of the level difference spectrum is known. The reason for this is obvious: in case the direct deduction of the impedance is carried out, one complex value, the surface impedance, has to be deduced from a single – possibly not even complex - value of the level difference spectrum at each frequency. On the other hand, for estimation of the absorber parameters (often two parameters are sufficient), the whole level difference spectrum with a potentially high number of frequencies is available. In addition, the latter procedure can benefit from the fact that some (geometry dependent) frequency ranges (“ground dip”) are more sensitive to changes in the surface impedance than others. However, it is not guaranteed that the chosen absorber model predicts the ground impedance correctly in the low frequency range.

### Phase gradient method

In trying to improve the accuracy of surface impedance estimating from sound pressure measurements it has been proposed to measure the sound pressure not only at one or two locations but to use a pair of microphones to sample the pressure gradient [33] or, preferable, the phase gradient at different heights above the surface. The phase of the sound pressure gradient does show a pronounced change with height over the surface depending on surface impedance and frequency, even at low frequencies. An example is shown in figure 5. The method has been employed to determine under laboratory conditions for materials with low flow resistivity in the frequency range from 250 to 4000 Hz [34] assuming plane wave like reflection. The surface impedance is obtained by choosing the one that gives the best least-mean-square fit between model prediction and measurement. An attempt was made to use this procedure [35] for measuring above grass covered ground below 300 Hz showing a reasonable course of the impedance. In this case, the “exact” sound field above an impedance plane was taken into account. However, it is difficult to benchmark the results as they only agree in part with the Delany-Bazley one-parameter model and measurements from other authors [36] in that frequency range. The phase gradient method, while having the potential to be capable of low frequency measurements, has a number of drawbacks preventing their use for routine measurements. The measurement of the pressure gradient at a lot of positions above the surface is time consuming and assumes stationary propagation conditions. Furthermore, it is preferable that the gradient is measured up to heights equal to the wavelength which means that a large set-up is needed for low frequencies: The authors [35] placed the sound source at a height of seven meters above the ground. Finally, this method has only been used, with an adequate sound field model, for normal incidence and it's performance for other angles of incidence is unknown.

Remark: while data in the frequency range of 60 – 290 Hz for uncultivated grassland and normal incidence is presented in [36], a prototype device has been used in this investigation. It is based on a volume velocity source (mechanically driven piston with known deflection) exiting a cylindrical cavity which is placed on the ground. By measuring the sound pressure in the cavity, the impedance is obtained (the cylinder is small enough not to allow wave propagation). An extensive calibration is necessary to account for the admittance of the device itself and the imperfect seal between device and surface. The set-up has found no distribution hereafter and will therefore not be discussed in this work.

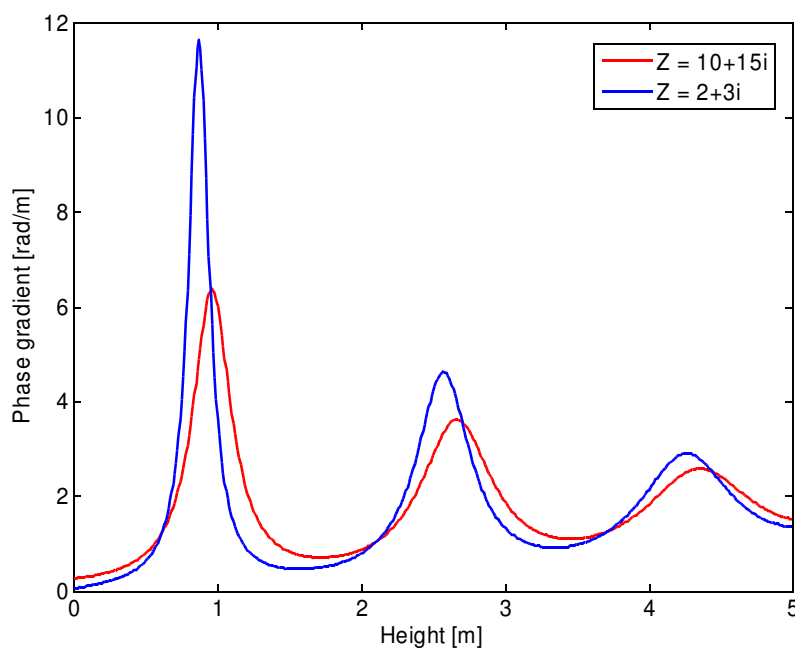


Figure 5: Phase gradient versus height above an impedance plane for a source height of 7 meters, a frequency of 100 Hz and a normalised surface impedance of  $10 + 15i$  and  $2 + 3i$ .

### Single microphone: Excess attenuation

An alternative to using a pair of microphones is to evaluate the excess attenuation by a single microphone. This requires a reference measurement in a free field to get the direct sound pressure spectrum which is compared (eq.8) with the spectrum including the ground reflections (“total sound pressure”), thus the course of action is similar to the subtraction technique for the pulse-echo method. Figure 6 shows an example of an excess attenuation spectrum with the same geometry used for figure 4, the single microphone being at the upper microphone's position 0.46 meters above the ground. The need for the reference measurement is the weak point of this method. Precise results can only be expected if both measurements are done under the same conditions. While this is typically not a problem indoors, it means that for outdoor use the reference measurements should also be done outdoors and not in an anechoic room to avoid problems arising from the effect of a different environmental temperature and humidity on the speed of sound and microphone sensitivity. The source then has to be positioned high above the ground and the unwanted ground reflection will be removed in the time domain requiring a system capable of measuring the impulse response and not only a spectrum or transfer function. Further uncertainties remaining are minor differences in the source-receiver distance between the two measurements leading to a phase error in the EA spectrum, though a possible delay between the two signals can easily be detected by cross correlating them. A general problem is the fact that reference and total sound pressure are not collected at the same moment in time. Propagation conditions may change in the meantime, e.g. by change of wind direction and speed or degree of turbulence, leading to a (slightly) inaccurate EA spectrum.

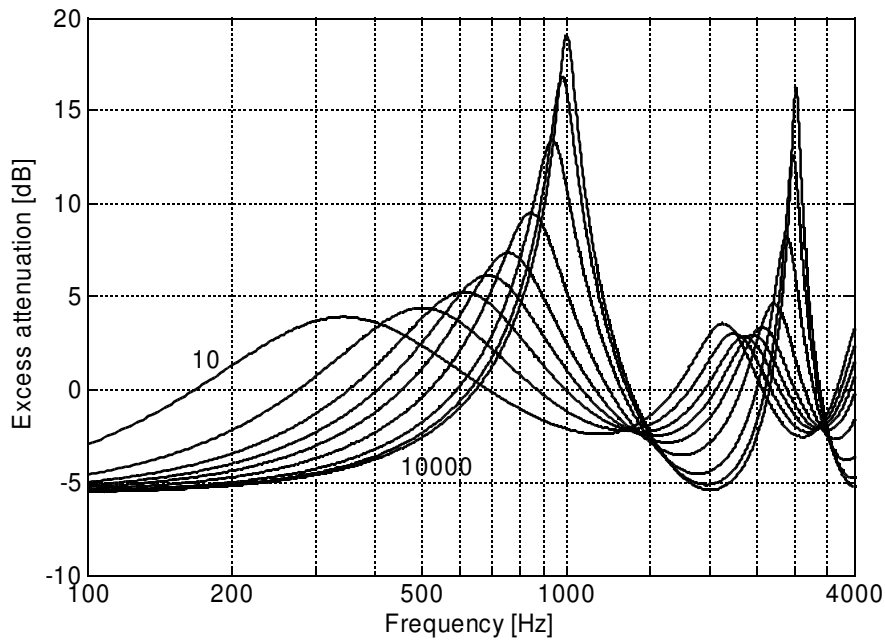


Figure 6: Excess attenuation versus effective flow resistivity (from 10 to 10,000 krayl/m) of the Delany-Bazley absorber model. Geometry A from ANSI S1.18 (upper microphone).

### Level difference versus excess attenuation

It is helpful to compare the level difference spectrum in fig.4 and the excess attenuation spectrum presented in fig.6 in order to assess which of the two methods may be more favourable for the low frequency range below approx. 500 Hz.

Both spectra are comparable in shape and partly in scale and will become even more similar if the level difference is measured with one microphone on the ground [37] where it is not subject to interference effects between incident and reflected wave. An excess attenuation spectrum is shaped by these effects: for the given geometry, destructive interference will occur near 1 kHz and 3 kHz whereas constructive interference is anticipated near 2 kHz. The highly reflecting ground with a flow resistivity of 10,000 krayl/m follows this prediction well. The lower the impedance becomes, the less pronounced the excess attenuation spectra will be and an additional shift of the extrema towards lower frequencies is observed.

A general weakness of the transfer function technique is revealed by figure 4: the level difference at low frequencies will not depend much on the surface impedance. It is therefore not well suited for low frequency measurements without further improvements. On the other hand, the excess attenuation shows a higher change with impedance in the low frequency range. Table 12 gives an overview of the change in excess attenuation EA and level difference LD/LD<sub>0</sub> if the flow resistivity is changed from 10 to 10,000 krayl/m and from 100 to 1,000 krayl/m. On average, the change will increase with increasing frequency and be largest in the excess attenuation. If one concentrates on flow resistivities between 100 and 1,000 krayl/m typically of most naturally occurring grounds, one notices that the level difference shows a comparable sensitivity if one microphone is placed on the ground (LD<sub>0</sub>). Even though, up to now, only one geometry has been considered it appears likely that the two microphone technique can offer a similar sensitivity to changes in the surface impedance for low frequencies avoiding the drawbacks associated with the excess attenuation measurement.

	10 / 10,000 krayl/m			100 / 1,000 krayl/m		
	EA	LD	LD <sub>0</sub>	EA	LD	LD <sub>0</sub>
100 Hz	2.5	0.6	1.3	0.3	0.1	0.3
250 Hz	7.7	1.9	4.3	1.4	0.5	1.1
500 Hz	5.3	4.1	9.5	4.2	1.4	3.1

Table 2: Change, in dB, of excess attenuation EA and level difference for two values of the flow resistivity of the ground (Delany-Bazley model). Level difference for geometry A (LD) and geometry A with lower microphone on the ground (LD<sub>0</sub>).

### Field impedance based

The field impedance, like excess attenuation and pressure transfer function, is one of the parameters of a sound field not depending on the source strength and hence being suitable for surface impedance estimation by sound field matching. Though it may seem surprising, the field impedance, being a quantity that could not be measured directly for a long time, was one of the first parameter used for that purpose.

### Two microphone impedance probe

Using a pair of two closely spaced microphones comparable to an intensity probe, the sound velocity can be determined (finite difference approximation of the pressure gradient) from the sound pressures at the two microphone positions with distance  $\Delta r$  [38]:

$$u = \frac{1}{i\omega\rho_0\Delta r}(p_2 - p_1), \quad p = (p_2 + p_1)/2 \quad (15)$$

Equation 15 can be rewritten with the transfer function  $H_{12}$  to obtain the (normalised) field impedance  $Z_{MP}$  at the midpoint between the microphones at height  $d$  above the surface:

$$Z_{MP}(d) = \frac{1}{Z_c} \frac{p}{u} = \frac{1}{2} i k \Delta r \frac{1 + H_{12}}{1 - H_{12}} \quad (16)$$

It was common practice to assume plane wave reflection so that the surface impedance can be calculated analytically from the field impedance (eq.17 for normal incidence plane waves).

$$Z = \frac{Z_{MP} - i \tan(kd)}{1 - i Z_{MP} \tan(kd)} \quad (17)$$

A similar equation is known for spherical waves with plane wave like reflection [39].

The technique has been very popular as it only requires a transfer function to be measured and applies only simple mathematical calculations.

Agreement of the measurement results with Kundt's tube data has been reported [40] for frequencies larger than 700 Hz in an anechoic environment. Later studies [39] indicate a lower frequency limit of 500 Hz for an anechoic environment and 1 kHz for a large non-anechoic room with poor results in smaller reverberant rooms. The limited success in measuring below 500 Hz, even in a free field, led to an optimisation of the procedure [41]. Pure tones were used and the distance between the microphones was increased bearing in mind the small pressure gradient at low frequencies.

Furthermore, it was suggested to calibrate the microphones by placing them next to each other at a distance of several meters from the loudspeaker so that the sound pressure at their positions is equal. These improvements made surface impedance measurements down to 250 Hz – in a free field for normal incidence – possible.

Parameters influencing the accuracy of the two microphone field impedance method have been thoroughly analysed [42]. These include the finite difference approximation of the sound pressure gradient leading to errors for higher frequencies. Phase errors of the microphones (or other parts of the equipment) reduce the low frequency performance demanding higher microphone separations and

preferably phase-matched microphones. Other uncertainties include the distance between the acoustical centres of the microphones, the distance of the surface to the midpoint between them and the plane wave hypothesis. The authors conclude that in a real life situation a reasonable performance can be expected between 300 Hz and 8 kHz for materials with low flow resistivity (10 krayl/m), while the method is not recommended for hard surfaces (1,000 krayl/m).

One may wonder why this method has been used at all because, except from the equations used - but assuming the same sound field model - it is identical to the two microphone transfer function method meaning that eq.14 could be used. A comparison between the two evaluation methods [43] reveals that indeed the latter method is superior because it does not rely on the finite difference approximation used to derive the field impedance at the midpoint between the microphones. It offers reasonable accuracy between 300 and 5000 Hz for absorbent surfaces and angle of incidence of up to 30° from normal.

### Microflown based PU probe

With the invention of the microflown in 1994 and its commercial availability in 1997 it was for the first time possible to measure the particle velocity directly. Combined with a small microphone it is possible to create a sensor (called "PU probe" by the manufacturer) which can measure pressure and velocity at (almost) the same location and hence provides the sound intensity and field impedance. A PU probe can be used in different ways to determine the surface impedance of materials. The most straightforward approach would be to measure the field impedance directly at the surface and consider the result to be the surface impedance. However, as was already mentioned, this is only true for an incident plane wave and high errors can be expected for low frequencies and/ or the source being close to the surface ( $k \cdot R$  not much larger than unity). Another problem is the fact that, though the PU probe is small, it can not measure directly at the surface. Unfortunately, the gradient of the field impedance is high near the surface, especially for materials with high impedance, so that even a distance of a few millimetres causes significant deviations as long as  $k \cdot R$  not much greater 1, even for normal incidence [44].

The PU probe can, just like a two microphone impedance probe, be used for sound field matching. This as first suggest by [45] using a simple mirror source model. The results appear to be promising and agree reasonably well with results from the Tamura method and predictions by the Biot-Allard-Johnson model. Agreement in the lower frequency range, however, is limited and influenced by the angle of incident. The poor performance of this procedure is also demonstrated by measurements on small samples often leading to unrealistic absorption coefficients below approx. 700 Hz [46]. One reason is the approximations used for the calculation (plane wave like reflection). As shown in [44], it is expected that errors result from this approximation for low frequencies unless the PU probe is positioned very close to the surface (5 mm). Positioning the sensor close to the surface, though suggested by the simulation results, is problematic in practise. Near the surface, the velocity will be close to zero for materials with a high impedance typically occurring at low frequencies. Thus, the sensor has to be positioned further away from the surface leading to increasing errors due to the sound field approximation.

Apart from these physical problems, microflowns have other disadvantages. The price is higher compared to precision microphones (approx. three times) while not offering the dynamic range and low self-noise one may be accustomed to, though the improvements during the last ten years are significant. Another problem is the calibration: micoflowns exhibit a distinct change of sensitivity with frequency which is only partly corrected by manufacturer provided equalizer. A broadband calibration, either in a free field or a standing wave tube, is required instead of the single frequency calibration sufficient for microphones.

Finally, it is unknown if a PU probe does offer an advantage over using a pair of microphones. However, one recent study [47] is promising. It employs one advantage of microflowns, their dipole-like directivity pattern. If it is orientated tangential to the (spherical) wave front, it will not detect any particle velocity in a free field (fig.7). If placed above a reflecting surface, the microflown will "see" the mirror source. The reflection coefficient can be determined by comparing the velocity found with the material sample with the velocity generated by an totally reflecting surface. If the geometry is kept constant, the reflection coefficient is simply the ratio of the two velocities. This procedure may therefore offer a method of investigation high impedance surfaces while not fit for materials with low reflection.

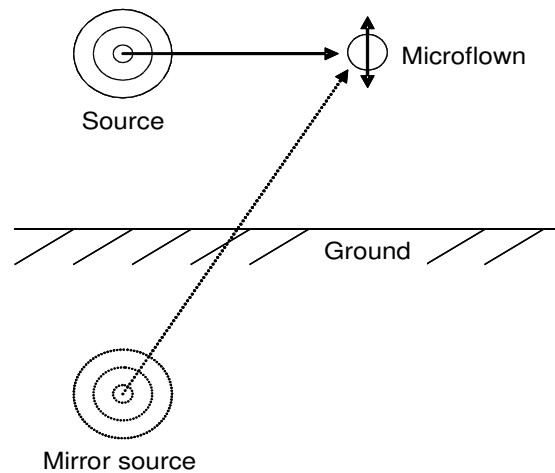


*Figure 7: Reflection coefficient measurement with a microflown orientated in a way that it only detects the velocity originating from the mirror source.*

### Summary: In-situ impedance measurement

A variety of methods for in-situ surface impedance measurements have been presented in this chapter. They differ largely in the effort need (concerning both lead time and needed equipment) as well as in their applicable frequency and surface impedance range.

Currently most widespread is the standardised pulse-echo method based on their simple set-up and easy to understand theoretical basics. It is well suited for higher frequencies (above about 500 Hz) and incident angles not too far from normal.

If one has a microflown available it is as well possible to directly measure the field impedance close to the surface which is a good estimator of the surface impedance as long as  $k \cdot R \gg 1$ .

For lower frequencies and near grazing angles of incident, indirect methods with an appropriate sound field model are inevitable.

The two-microphone / transfer function method has the potential to become widely used, especially if being standardised, having the advantage that no reference measurement is needed hence changes in time of the propagation conditions have no influence. However, the performance below 300 Hz is still not very convincing and further investigations to analyse the reason for this are needed to improve the method.

Only two techniques are known which have shown acceptable performance for lower frequencies. The phase gradient method uses only simple and readily available equipment but requires a large set-up and is time consuming.

A promising approach is the use of a microflown particle velocity sensor orientated in a way that it will not pick up any signal in a free field but "sees" just the reflection. This method appear to be especially fit for high impedance materials, which, as will later be shown, are challenging for the two microphone method. Unfortunately, experience with this method is very limited and restricted to a controlled laboratory environment so that it's suitability for outdoor applications is yet unknown.



## VII. Sound field models

Any of the discussed indirect methods do rely – at least in theory – on a sound field model which is used for choosing a surface impedance that matches the measured and predicted quantity of the sound field, e.g. excess attenuation or field impedance.

### Sound field above an infinite locally reacting impedance plane

A commonly used and thoroughly validated model [48] for the sound field above an impedance plane will now be presented. The model assumes local reaction (discussed later) and an infinite plane of constant impedance.

#### The Nobile&Hayek solution

The sound field above a medium of finite impedance has long been of interest. The actual formulation of the problem is trivial; cylindrical coordinates - radial distance  $R$  and height above the surface  $z$  – will be used taken in mind the rotation symmetry of the problem and an  $\exp(-i\omega t)$  time dependency is assumed.

Let there be a point source of unity strength in a free space with wave number  $k$  at position  $R=0$  and  $z=h_s$ . The velocity potential is given by eq.18.

$$(\nabla^2 + k^2)\phi(R, z) = -\frac{2}{R}\delta(R)\delta(z-h_s) \quad (18)$$

The solution of eq.18 are ordinary spherical wave originating from  $(0, h_s)$ . The existence of an impedance plane at  $z=0$  places a boundary condition on the system expressed by eq.19. This boundary condition implicitly includes the assumption of local reaction.

$$\frac{\partial \phi(R, 0)}{\partial z} + ik\beta\phi(R, 0) = 0 \quad (19)$$

The way of finding the solution for the velocity potential  $\Phi$  from this pair of equations is far from trivial and of no interest here. The reader is referred to the correspondent literature [e.g. 49]. The exact solution is given by eq.20.

$$\phi(R, z) = \frac{1}{r_1} e^{ikr_1} + \int_0^\infty \left( \frac{\nu + ik\beta}{\nu - ik\beta} \right) \frac{e^{-\nu(z+h_s)}}{\nu} \Lambda J_0(\Lambda r) d\Lambda \quad \text{where } \nu^2 = \Lambda^2 - k^2 \quad (20)$$

This integral representation is of little practical use as conducting the integration is impaired by the existence of a pole at  $\nu = +ik\beta$  and branch points at  $\Lambda = \pm k$ .

Only in individual cases a simplification is possible, so one has to deal with approximations (it is, however, possible to rewrite eq.20 as a real integral which allows for numerical integration). By assuming that  $k \cdot r_1$  is much larger than unity, the integral can be transformed into an asymptotic series (a Taylor series expansion integrated beyond its radius of convergence). The result is found in eq.21 to 29.  $r_1$  and  $r_1'$  are the lengths of the direct and reflected path,  $\theta$  the angle of incidence relative to the surface and  $R_p$  the plane wave reflection coefficient (eq.4).  $\text{erfc}()$  denotes the complementary error function and  $w()$  the Faddeva (complex error) function.

Equation 21 gives two different representations of the sound field, the so-called F-term and Q-term solution. The Q-term solution describes the sound field as the sum of the direct wave and a wave originating from a mirror source at  $(0, -h_s)$  with the spherical reflection coefficient  $Q$ . The F-term solution allows for an even better comparison with plane wave reflection theory. The total field is now the direct wave, a wave reflected with the plane wave reflection coefficient and a correction term ("ground wave") qualifying the deviation from plane wave like reflection. The function  $F$  is called boundary loss function.

$$\phi(R, z) = \frac{1}{r_1} e^{ikr_1} + Q \frac{1}{r_1'} e^{ikr_1'} = \frac{1}{r_1} e^{ikr_1} + R_p \frac{1}{r_1'} e^{ikr_1'} + (1 - R_p) F \frac{1}{r_1'} e^{ikr_1'} \quad (21)$$

$$r_1 = \sqrt{(h_s - z)^2 + R^2}; r_1' = \sqrt{(h_s + z)^2 + R^2}; \theta = \tan^{-1} \frac{h_s + z}{R} \quad (22)$$

$$F = 1 + \sum_{n=0}^{\infty} T_n (e_0 E_n + K_n) \quad (23)$$

$$T_n = \sum_{k=0}^{(n-2k)>0} \binom{n-k}{k} a_{n-k} \left( \frac{4G}{H} \right)^{n-k} \quad (24)$$

$$E_0 = 1, E_1 = -\frac{1}{2}, E_m = -\frac{1}{2} E_{m-1} - \left( \frac{(m-1)}{8ikr_1' G} \right) E_{m-2} \quad (25)$$

$$K_0 = 0, K_1 = -\frac{1}{2}, K_m = -\frac{1}{2} K_{m-1} - \left( \frac{(m-1)}{8ikr_1' G} \right) K_{m-2} \quad (26)$$

$$G = 1 + \beta \sin \theta - \sqrt{1 - \beta^2} \cos \theta \quad (27)$$

$$e_1 = i\sqrt{\pi} \lambda e^{-\lambda^2} \operatorname{erfc}(-i\lambda) = i\sqrt{\pi} \lambda w(\lambda) \quad (28)$$

$$\lambda = \sqrt{ikr_1'} \sqrt{1 + \beta \sin \theta - \sqrt{1 - \beta^2} \cos \theta} \quad (29)$$

It is worth to look for simplifications of the above equations. The asymptotic series (eq.24) converges rapidly (but will diverge for a large number of terms) so it is sufficient to use the first term (n=0) of the series for many cases of practical interest. Equation 23 becomes eq.30 ("first term only solution"). Additionally, for small angles of incidence and high impedances, it is possible to replace the numerical distance  $\lambda$  by the definition provided by eq.31 [50].

$$F_1 = 1 + i\sqrt{\pi} \lambda w(\lambda) \quad (30)$$

$$\lambda = \sqrt{\frac{1}{2} ikr_1'} (\sin \theta + \beta) \quad (31)$$

### Examples

To receive an impression of how the sound field above a locally reacting impedance plane looks like, two examples shall be provided. Figure 8 and 9 show the relative sound pressure and vertical velocity at 100 Hz above a surface with an impedance of  $10 + 15i$ . Likewise, in figures 10 and 11, the same situation is depicted for a frequency of 1 kHz and an impedance of  $2 + 3i$ . Especially noteworthy is the standing wave which develops at 1 kHz with its alternating minima and maxima of pressure and velocity between source and surface and a (local) pressure maximum and velocity minimum at the surface.

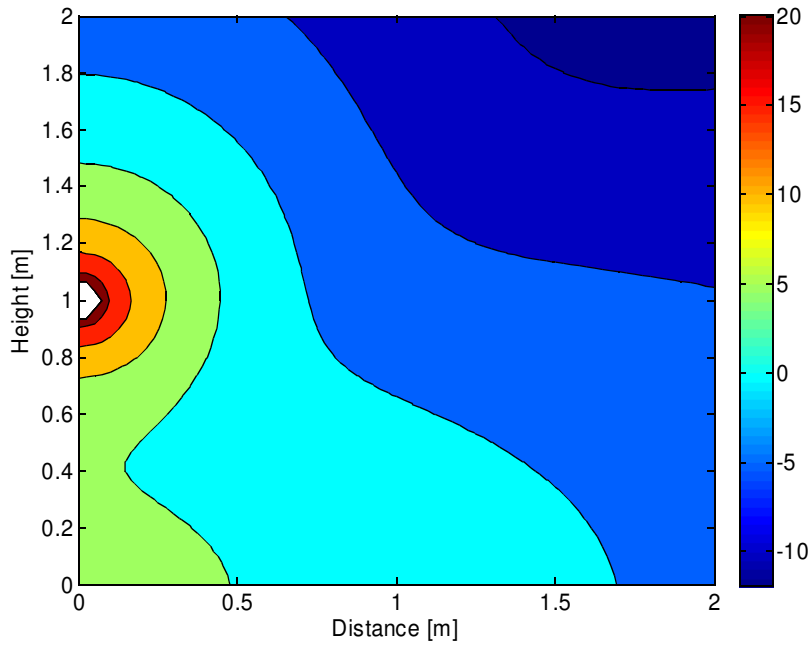


Figure 8: Sound field above a locally reacting impedance plane at 100 Hz. Sound pressure in dB re. free field @ 1 m. Surface impedance =  $(10 + 15j)$ . Source height is 1 m.

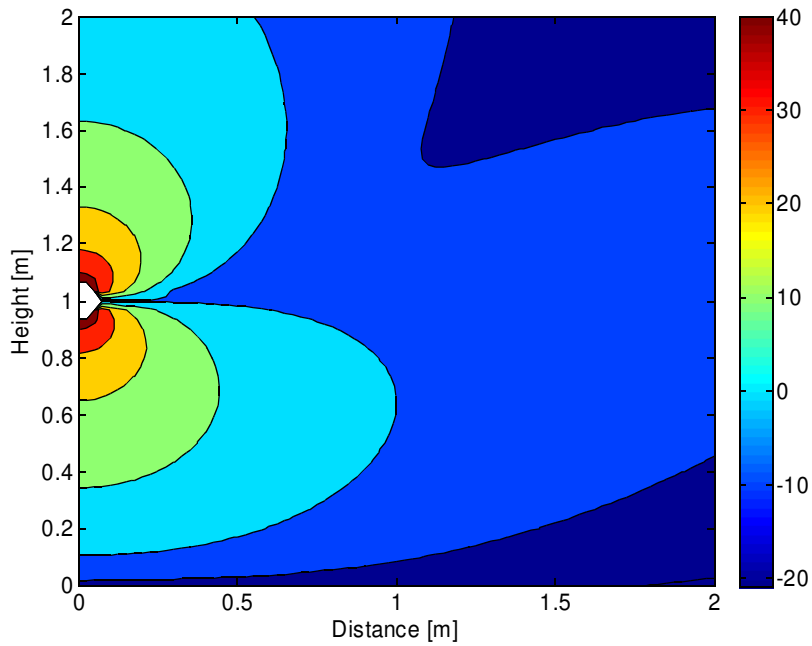


Figure 9: Sound field above a locally reacting impedance plane at 100 Hz. Vertical velocity in dB re. free field @ 1 m. Surface impedance =  $(10 + 15j)$ . Source height is 1 m.

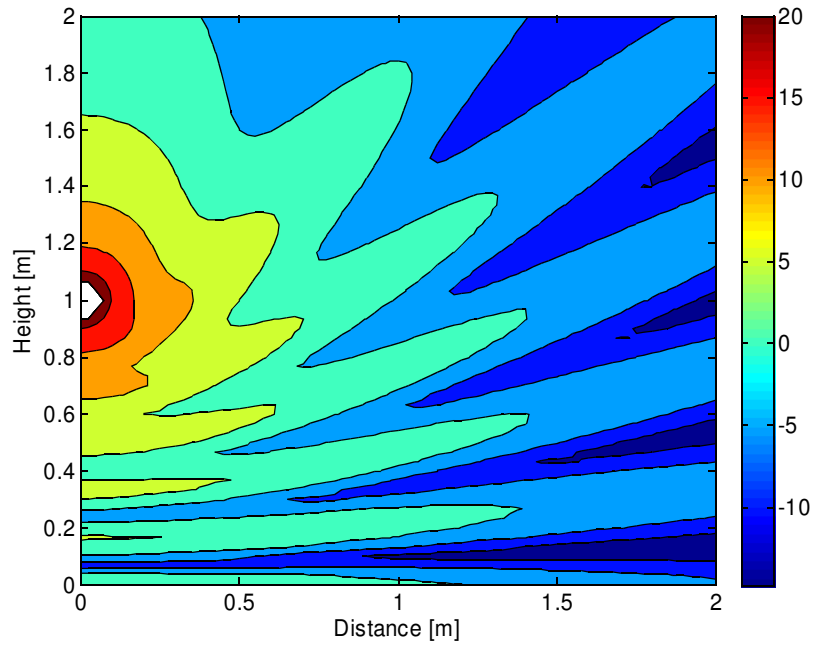


Figure 10: Sound field above a locally reacting impedance plane at 1 kHz. Sound pressure in dB re. free field @ 1 m. Surface impedance =  $(2 + 3i)$ . Source height is 1 m.

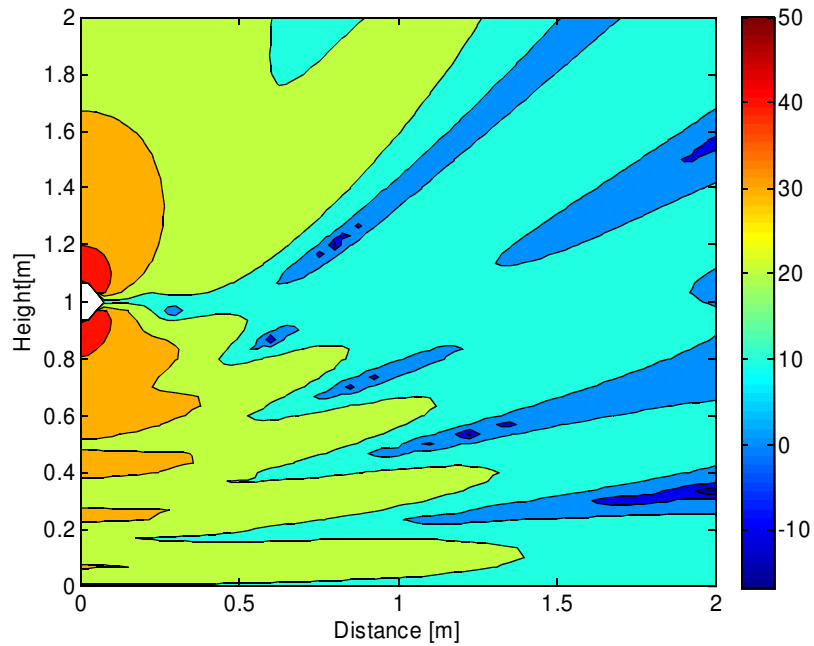


Figure 11: Sound field above a locally reacting impedance plane at 1 kHz. Vertical velocity in dB re. free field @ 1 m. Surface impedance =  $(2 + 3i)$ . Source height is 1 m.

## Special cases

Some special cases are of interest:

Normal incidence: for perpendicular incidence, an exact solution can be derived from eq.20,  $Ei()$  being the exponential integral:

$$\phi(R, z) = \frac{1}{r_1} e^{ikr_1} + \frac{1}{r_1'} e^{ikr_1'} - 2ik\beta e^{-ikr_1'\beta} Ei(ikr_1'(1+\beta)) \quad (32)$$

Grazing incidence: on grazing incidence, the plane wave reflection coefficient becomes -1 independent of the surface impedance and the total sound field is given by eq.33.

$$\phi(R, z) = 2F \frac{1}{r_1} e^{ikr_1} \quad (33)$$

The sound field is defined by the ground wave term; the assumption of plane wave like reflection would result in a sound pressure of zero ("plane wave paradox").

Large  $k \cdot r_1'$ : for large values of  $k \cdot r_1'$ , the boundary loss function  $F$  becomes zero and eq.21 is reduced to the plane wave like case:

$$\phi(R, z) = \frac{1}{r_1} e^{ikr_1} + R_p \frac{1}{r_1'} e^{ikr_1'} \quad (34)$$

This is the sound field description routinely employed by most users of in-situ reflection coefficient measurement procedures, as mentioned beforehand, because eq.34 can be solved analytically for the surface impedance.

## Effect of the approximations

At this point, the attentive reader may remark that the assumptions being applied to derive eq.30 and 31 are quite extensive and make the general use of these approximations questionable. Fortunately, if dealing with typical ground impedances which are high at low frequencies, the approximate solutions are usually indistinguishable from those of the more exact expressions [51]. We shall have a closer look at the situation.

The asymptotic series rarely differs from the exact solution (eq.20) although it is based on the assumption  $k \cdot r_1' \gg 1$  [48]. For not too small surface impedances (e.g.  $Z = (2 + 3i)$ ), it will be practically identical to the exact solution for  $k \cdot r_1' > 0.1$ , even for near grazing incidence. Only for very low impedances (e.g.  $Z = (0.3 + 0.5i)$ ) one has to anticipate differences between asymptotic series and the exact solution for  $k \cdot r_1' < 3$  (depending on the angle of incidence), because the series does no longer converge, so that the first term only solution (eq.30) can be an even better choice.

A comparison of the reflection coefficient given by the plane wave approximation ( $R_p$ ), the first term only solution ( $Q_1$ ) and the spherical reflection coefficient calculated with the asymptotic series with  $n=5$  ( $Q_5$ ) is shown in fig.12. It is evident that the difference between  $Q_1$  and  $Q_5$  is very low in the whole frequency range, especially above 100 Hz ( $k \cdot r_1' \approx 4$ ). The plane wave reflection coefficient, on the other hand, differs significantly from the spherical wave reflection coefficient for frequencies below 1 kHz. Comparisons for different geometries and surface impedances [48] underline this trend. Hence, it is strongly recommended to mind the ground wave (eq.21) when calculating the sound field above an impedance plane because of the possible high deviations from the plane wave like case. This is especially true for (near) grazing incidence for which plane wave theory predicts a sound pressure of zero. On the other hand,  $R_p$  is generally a good estimator for  $Q$  in case of near normal incidence. What remains is the approximation for the numerical distance. In fig.13, the spherical wave reflection coefficient  $Q$  (first term only solution, eq.30) is shown for geometry A ( $\theta = 24^\circ$ ) and three flow resistivities. Even for an unusually low flow resistivity (and hence impedance) of 1 krayl/m the approximation has hardly any effect. It is not recommended for near normal incidence, though, as the difference between "exact" and approximate numerical distance will increase.

In this work, the first term only solution in combination with the approximation for the numerical distance will be used, as suggested by ANSI S1.18. This is justified by the fact that outdoor grounds, with very few exceptions, have a high impedance at low frequencies. Furthermore, measurements were done with small angles of incidence.

Suitable approximations for the Faddeeva function can be found in textbooks [52]. For the programming language C + + , a fast implementation is available in the Matpack<sup>1</sup> package. A Matlab port of this algorithm has been used for the calculations in this work.

A comparable sound field model for a dipole source has been suggested [53] but is of no relevance to this work because of the limited low frequency performance of a dipole source.

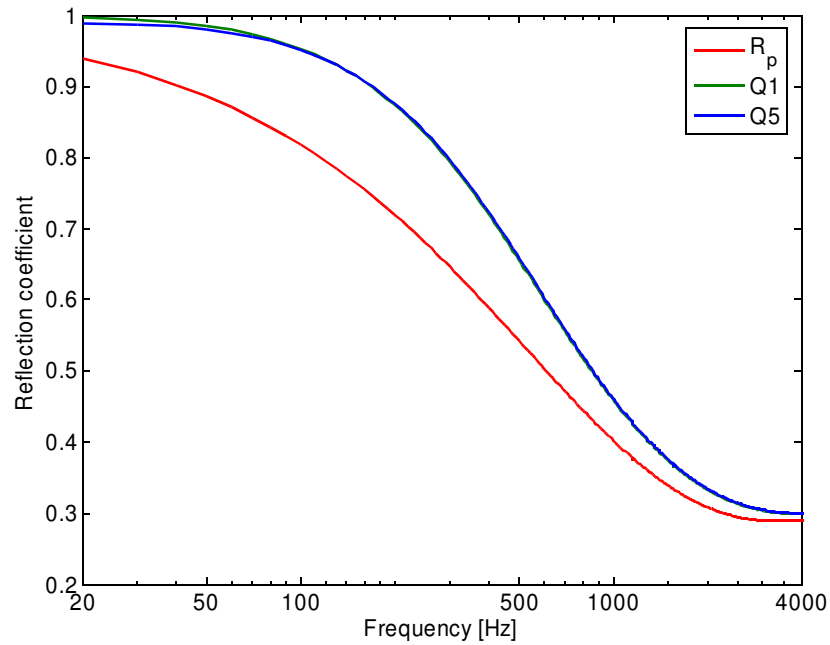


Figure 12: Comparison of plane wave ( $R_p$ ) and spherical reflection coefficients ( $Q_1 / Q_5$ ) for geometry A from ANSI S1.18 (upper microphone) and a locally reacting ground with a flow resistivity of 100 krayl/m (Delany-Bazley model).

<sup>1</sup> www.matpack.de

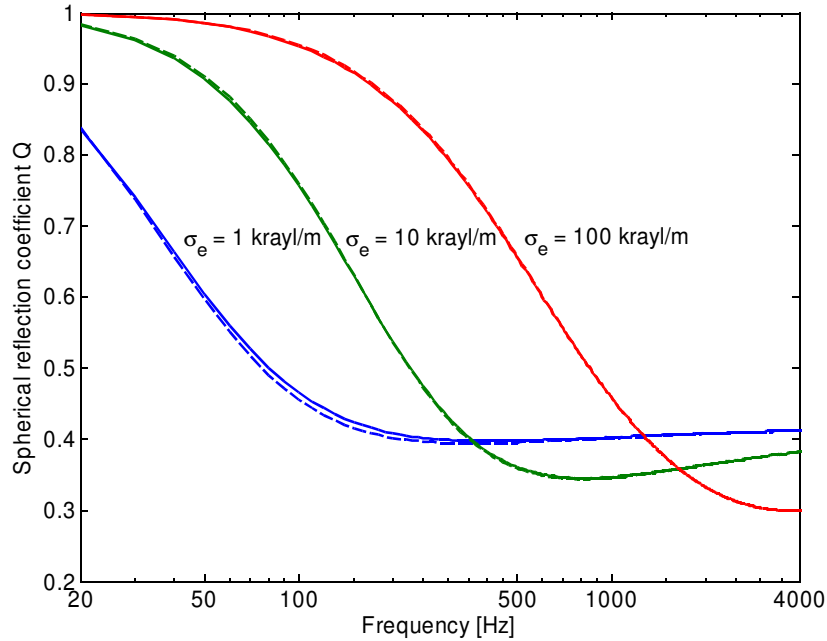


Figure 13: Comparison of the spherical wave reflection coefficient  $Q$  using the exact numerical distance (—) (eq.29) and it's approximation (---) (eq.31). Geometry A (upper microphone) and DB model with three flow resistivities.

The sound field description presented applies only to a – potentially rare – case, a locally reacting, smooth and infinite plane of constant impedance. These are obviously not properties of naturally occurring grounds. Thus, it should be judged what consequences deviations from these assumptions have. We will concentrate on two phenomena: extended reaction and rough surfaces.

### Local and extended reaction

The Nobile&Hayek model as well as the standard equation for calculating the plane wave reflection coefficient (eq.4) assume local reaction. Local or point reaction can be depicted in two ways: viewed from the outside, a locally reacting material is marked by a surface impedance independent of the angle of incidence. The mechanism leading to this behaviour is the assumption that the refracted wave travelling in the material will propagate only normal to the surface and not laterally to it. This explains the expression “point reacting”. The reflection at one location on the surface is only depending on the properties at this location and is not influenced by what happens in the surrounding area.

Even without a mathematical model it is easy to spot, from geometrical considerations, the situations in which local reaction can be expected.

1. For near normal angles of incident.
2. For a high index of refraction or, in other words, for a low speed of sound in the medium compared to the speed of sound in air. For porous material this is equal to a high flow resistivity.
3. For a high propagation loss in the material. For anisotropic materials, if the propagation loss in lateral direction is much higher than the loss in normal direction.

For natural grounds, criteria 2 is of significance. Most grounds have flow resistivities of 100 krayl/m and above unlike fibrous absorbers or foams used for sound absorption in buildings, vehicles and machinery. It is therefore, in general, adequate to assume local reaction [51,54].

## Effective impedance

If the material does not show point reaction, this will change the sound field model as the surface impedance now depends on the angle of incident. Happily, it is not necessary to completely revise the model but a minor modification is sufficient. The only change is that the surface admittance  $\beta$  has to be replaced by the so-called effective impedance  $\beta_e$  [55], a function of two complimentary material parameters, the characteristic impedance  $Z_c$  and the wave number  $k'$  in the material. Two cases will be distinguished:

### Semi-infinite media

If the medium is of infinite thickness, the (normalised) effective admittance is given by eq.35.

$$\beta_e = m \sqrt{k'^2 - \cos^2 \theta} \quad (35)$$

### Layered media

For a layer of finite thickness  $d$  above a hard backing, eq.36 applies.

$$\beta_e = -i m \sqrt{k'^2 - \cos^2 \theta} \tan(k d \sqrt{k'^2 - \cos^2 \theta}) \quad (36)$$

where

$$m = \frac{\rho_0}{\rho_m} = \frac{1}{k'} \frac{1}{Z_c} \quad (37)$$

The index 0 marks the characteristics of air, index  $m$  the corresponding values for the material. Equation 35 confirms the criteria for a locally reacting ground. For normal incidence ( $\theta = \pi/2$ ), the effective impedance is equal to the characteristic impedance of the material. Likewise, for a low speed of sound, the wave number  $k'$  (or index of refraction) becomes large compared to  $\cos^2 \theta$  and the effective impedance is (nearly) angle independent. For thin layers, the situation is more complicated. For perpendicular incidence, the (normalised) effective impedance is (eq.38)

$$Z_e = i Z_c \cot(k_m d) \quad (38)$$

which is not necessarily equal to the characteristic impedance. This will only happen for large  $\text{Im}(k_m d)$  – the total propagation loss in the material - as  $\cot(k_m d)$  will converge to  $-i$ . For future validation of measurement results it is helpful to look at the differences between the effective surface impedance following from local or extended reaction. Two examples are given in fig.14 And 15. For a low flow resistivity of 10 krayl/m, the difference between the locally reacting and semi-infinite medium increases slowly with increasing frequency. The hard backed layer, on the other hand, has a significantly different impedance below approx. 500 Hz with an almost constant real part. For materials of higher flow resistivity, in this case 100 krayl/m, the effect of the extended reaction is negligible. These examples reveal what course of the surface impedance is to be expected. For grounds with high flow resistivity or thick layers of materials with low flow resistivity, the effective impedance will be similar to the characteristic impedance of the material with a continuous decrease of real and imaginary part with increasing frequency. Thin layers of materials with low flow resistivity, on the other hand, demonstrate a substantially different behaviour which is characterised by an almost constant real part of the impedance. Depending on the angle of incidence, thin layers will also show “ripples” in the impedance due to interference effects from the reflection at the bottom layer. The effective impedance is a convenient concept to “convert” the properties of a non-locally reacting medium into the equivalent impedance of a locally reacting surface which can subsequently be used to predict the sound field. On the other hand, the deduction of the material properties (characteristic impedance, wave number and layer thickness) from sound field quantities like pressure transfer function or field impedance is not as simple as deducting the effective impedance and will require measurements at different angles of incidence.



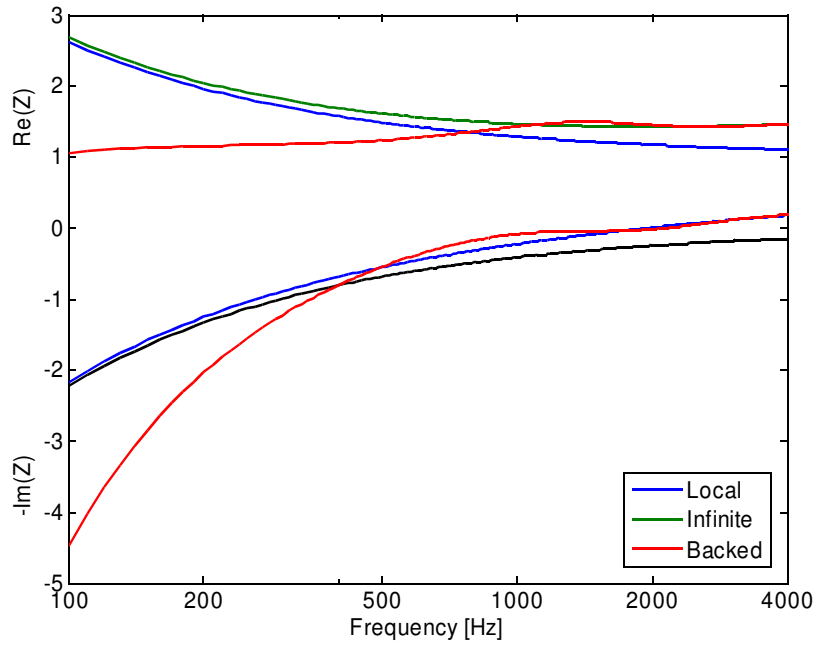


Figure 14: Difference in the effective surface impedance  $Z$  between local and extended reaction (semi-infinite or 10cm layer with hard backing) for a material with a flow resistivity of 10 krayl/m. Geometry A ( $\theta = 24^\circ$ ).

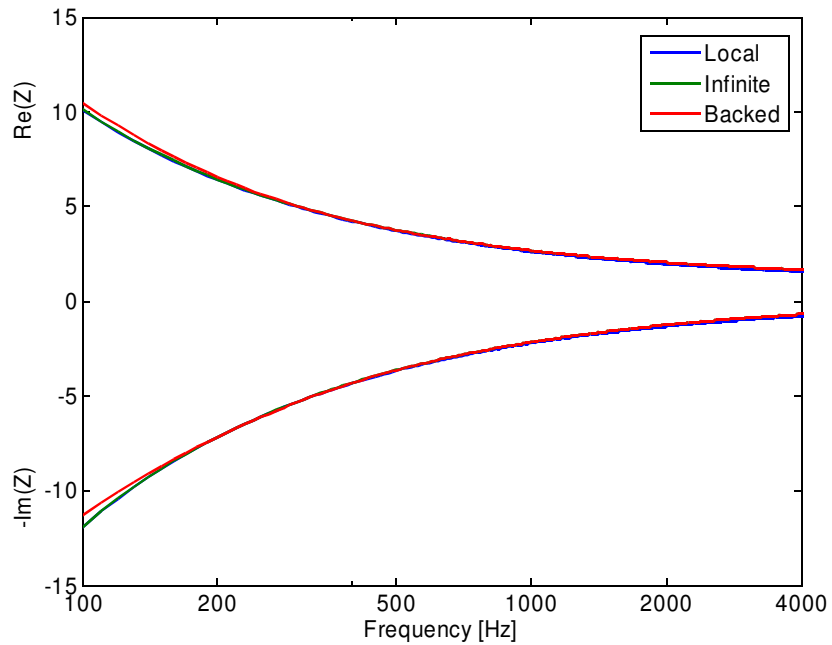


Figure 15: Difference in the effective surface impedance  $Z$  between local and extended reaction (semi-infinite or 10cm layer with hard backing) for a material with a flow resistivity of 100 krayl/m. Geometry A ( $\theta = 24^\circ$ ).

### Rough surfaces

Natural grounds rarely, if at all, have a smooth surface. Just like in the case of extended reaction, it is necessary to appraise the effect this roughness will have on the predicted surface impedance in comparison with a smooth surface of the same material. Fortunately, it is possible to describe a rough

surface by an equivalent effective surface impedance, too. An approximate solution is given by eq.39 for three-dimensional scatterers, with dimension and spacing small compared to the wave length, on a locally reacting smooth surface [56]:

$$\beta_e = -ik \frac{\sigma_v}{2} + \beta(1 - ik_m \sigma_v) \quad (39)$$

$k_0$  is the wave number in air,  $k_m$  the wave number in the material and  $\beta$  the normalised surface admittance of the smooth surface. The roughness parameter  $\sigma_v$  is the volume of the roughness elements per unit area of the surface, the average height.

The effect of the roughness is that the surface appears to have a lower impedance compared to a smooth surface of the same material. An example is provided in fig.16. The effect on the excess attenuation is the same as if the material had a lower flow resistivity: the minima and maxima are shifted towards lower frequencies and are less pronounced (fig.6).

An interesting note concerning measurements of the surface impedance of rough materials is given by [57]: the measurement results will agree best with the predictions by eq.39 if the reference plane for the geometry is placed at the top of the roughness elements.

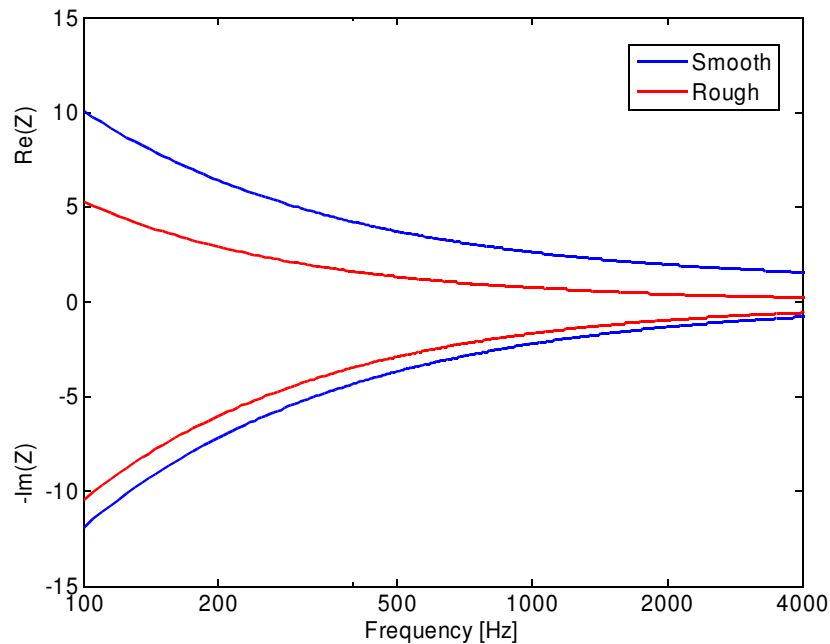


Figure 16: Comparison of the effective surface impedance of a smooth and a rough surface. DB model, effective flow resistivity 100 krayl/m. Mean roughness height is 1 cm.

## VIII. External influences

The sound field above an impedance plane is not only dependent on the acoustical properties of the ground, but there are a number of "external" influences one should take into account when trying to determine the ground impedance in-situ. In this chapter, we will discuss the effect of two phenomena: atmospheric turbulence and unwanted reflections. Both can severely influence measurement results and define requirements for the measurement conditions.

### Turbulence

The sound field model introduced in chapter 4 assumes, like most models, a homogeneous atmosphere in which the speed of sound is constant in time and space. In reality, however, turbulence originating from wind shear or temperature gradients will cause spatial and temporal fluctuations in the local speed of sound. For the sake of simplification, it will be presumed that these fluctuations are zero mean random variables, meaning that (more or less) permanent differences, e.g. from thermal layering of the atmosphere, will not be regarded. In this case, the sound pressure at one location of the sound field will show random fluctuations in amplitude and phase (in relation to the source signal). In a free field, though, these fluctuations will not affect the average sound pressure as we assumed zero mean distributions. To eliminate the influence of turbulence, all one has to do is choose an averaging time which is large compared to the period of the turbulence. Turbulence, unfortunately, has another effect on the sound field: it will decorrelate formerly correlated (e.g. originating from a single source) signals which are distant in space or time or which, while being measured at the same location and moment in time, have a different propagation path. Thus, the situation gets more complicated when reflections from a surface exist, because the sound field is now the superposition of the direct and reflected field. In absence of turbulence, both fields have a fixed relation in sound pressure and phase defined by the geometry and the reflection coefficient. This leads to the well known interference effects (fig.6) in the excess attenuation and level difference spectrum. Turbulence will, to some extent, destroy this fixed relation and create a less pronounced interference pattern, meaning that even the long time average sound pressure will deviate from the one observed in a homogeneous atmosphere. With certain assumptions it is possible to find a mathematical expression for the average (squared) sound pressure [58], expressed as mean excess attenuation  $\langle EA \rangle$  in eq. 40 - 43 [37].

$$\langle EA \rangle = -10 \lg \left( 1 + \frac{r_1^2}{r_1'^2} |Q|^2 + 2 \frac{r_1}{r_1'} |Q| \cos [k(r_1' - r_1) + \psi] T \right) \quad (40)$$

$$T = \exp[\alpha \sigma^2 (1 - \rho)], \quad \sigma^2 = \sqrt{\pi} \langle n^2 \rangle k^2 R L_0 \quad (41)$$

$$\rho = \rho_1 + \rho_2 = (\sqrt{\pi} L_0 / 4h_r) \operatorname{erf} [2R_1 h_r / (R L_0)] + (\sqrt{\pi} L_0 / 4h_s) \operatorname{erf} [2(R - R_1) h_s / (R L_0)] \quad (42)$$

$$\alpha = 0.5 \text{ for } L_0 \ll \sqrt{R/k}, \quad \alpha = 1 \text{ for } L_0 \gg \sqrt{R/k} \quad (43)$$

with the spherical wave reflection coefficient  $Q = |Q| \exp(i\psi)$ , the mean squared index of refraction  $\langle n^2 \rangle$ , the scale of turbulence  $L_0$  and the other symbols (geometry) as defined in fig.2.

Data for the two measures of the turbulence can be found in [59]; for low to medium turbulence,  $\langle n^2 \rangle$  will be in the range  $(5 - 10) * 10^{-6}$  and  $L_0$  1 - 2 m (near the ground).

The consequences for the template method, which estimates the surface impedance by fitting an excess attenuation or level difference spectrum to predictions derived by use of an absorber model, have been thoroughly investigated [37]. A strong turbulence has been assumed ( $\langle n^2 \rangle = 2 * 10^{-5}$ ,  $L_0 = 1$  m,  $\alpha = 1$  and  $\rho = 0$ ) and the excess attenuation with and without turbulence was compared for different source and receiver heights and a fixed distance between them of 1.75 m. An example is shown in fig.17. The lower the source and receiver heights are, the higher the frequency of the first interference minimum (ground dip) and the more the amplitude of the minimum is affected by turbulence. On the other hand (not shown), the frequency of the ground dip is most sensitive to changes in the surface impedance for near grazing incidence. Hence, the author concludes that it is

best to select a source and receiver height of 0.2 – 0.4 m for a source-receiver distance of 1.75 m (equal to an angle of incidence of 13 – 25°) to attain an optimal trade-off between sensitivity to ground impedance and undesirable sensitivity to turbulence effects. These considerations have influenced the creation of ANSI S1.18 (template method) in its choice of measurement geometries as well as its upper limit of the wind speed of 5 m/s.

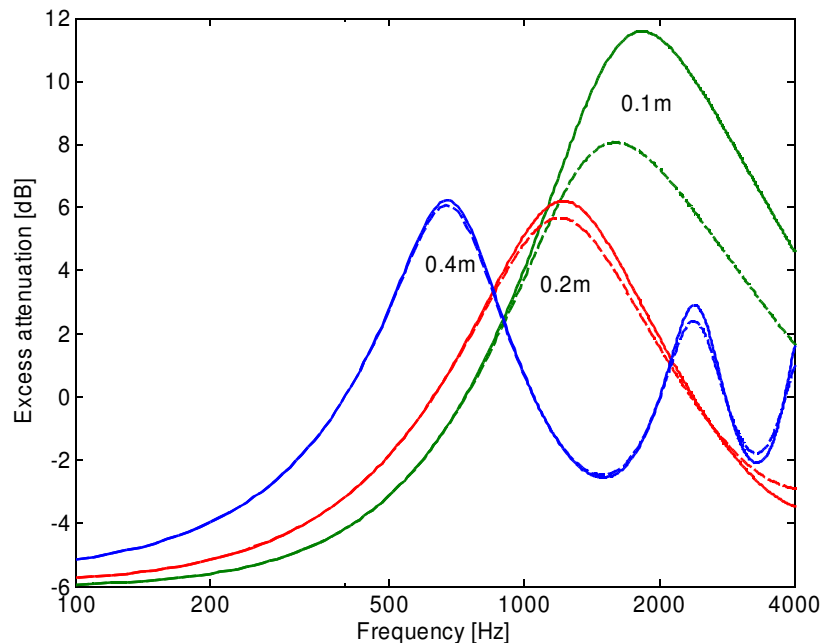


Figure 17: Effect of strong turbulence on the excess attenuation for three source and receiver heights  $h$  and a source-receiver distance of 1.75m. Impedance from Delany-Bazely model with an effective flow resistivity of 100 krayl/m. (—) without, (---) with turbulence.

Figure 17 shows that the region below 1 kHz is hardly affected by turbulence independent of source height. However, as will be demonstrated later, even small changes in the excess attenuation or level difference can have a severe influence on the predicted ground impedance at low frequencies if one tries to deduce it directly. Thus, it is worth having a closer look at this frequency range, this time for a “larger” geometry with a source height of 0.5 m, a source-receiver distance of 3 m and microphone heights of 0.05 and 0.95 m. Figure 18 shows the difference in excess attenuation with and without turbulence for strong ( $\langle n^2 \rangle = 2 \cdot 10^{-5}$ ,  $L_0 = 1$  m,  $\alpha = 1$  and  $\rho = 0$ ) and low/ medium turbulence ( $\langle n^2 \rangle = 1 \cdot 10^{-5}$ ,  $L_0 = 1$  m,  $\alpha$ ,  $\rho$  see eq.42, 43) in the frequency range 50 – 1000 Hz. The effect of low to medium turbulence is very low for both microphone positions and is of the magnitude of 0.02 dB. In comparison, strong turbulence can have a tenfold higher effect on the excess attenuation and consequently the level difference spectrum and may be a situation to be avoided for precise measurements below 1 kHz.

One has to be aware of equation 40 predicting the long time average excess attenuation, the instantaneous EA (or level difference) will show a certain degree of variability, an example is given in fig.19 for a five minute level difference measurement. This is always problematic if a measurement procedure requires two or more non-concurrent measurements to be made. Even if a long (“infinite”) averaging time is used it is not guaranteed that measurements done at different instants will lead to identical results compared to measurements done simultaneously, as the characteristics of the turbulence may change, e.g. due to changing wind speed or direction.

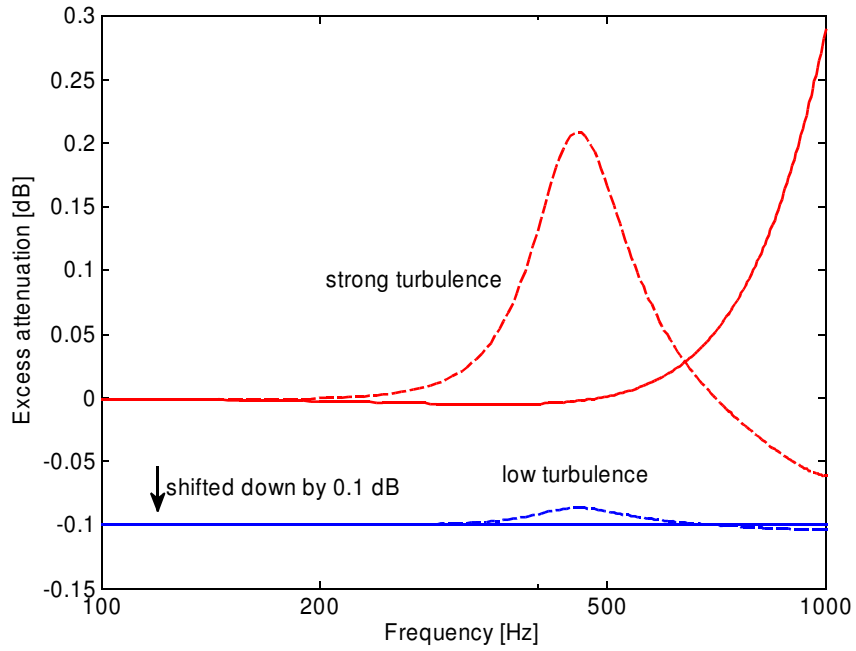


Figure 18: Effect of strong and low turbulence on the excess attenuation. Difference between EA with and without turbulence.  $R = 3$  m,  $h_s = 0.5$  m,  $h_{rl} = 0.05$  m (—) and  $h_{ru} = 0.95$  m (----). Effective flow resistivity = 100 krayl/m.

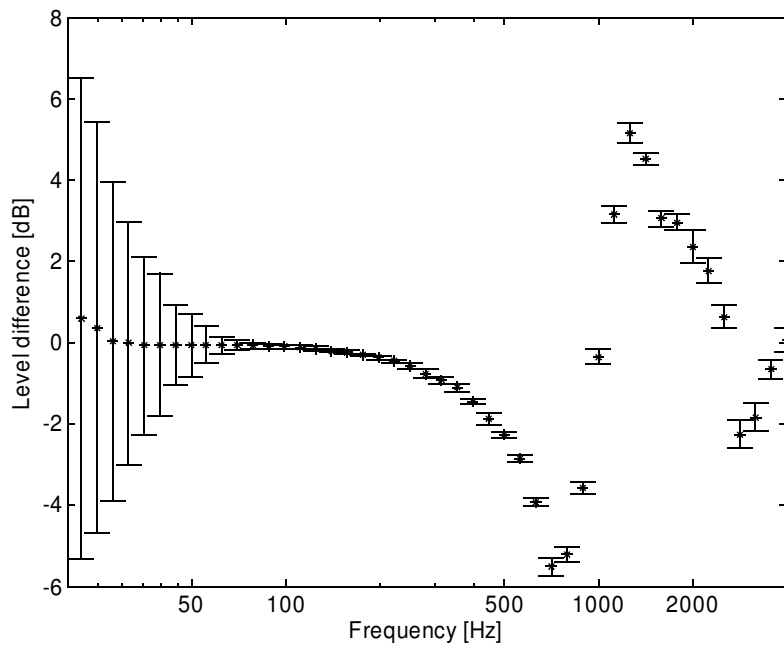


Figure 19: Variability of the level difference spectrum: mean level difference  $\pm$  standard deviation. Geometry A. Some background noise and wind speeds of 3 -4 (5) m/s. Sand area.

## Unwanted reflections

Any reflection not originating from the ground under test will, more or less, change the measured characteristic of the sound field and subsequently the predicted surface impedance. Sources of unwanted (parasitic) reflection can be buildings, natural obstacles (e.g. tree trunks) and finally the researcher and his/her equipment themselves. Reflections, in contrast to background noise, have the unpleasant property of being correlated with the source signal so that they are not suppressed by processing techniques like cross correlation of input and microphone signal. One solution is the use of a MLS analyser to determine the impulse response and use of a time window to gate the reflections. A certain delay between wanted and unwanted reflections will be necessary, nonetheless, as otherwise the window length will be too short and low frequency performance degrades.

It is best to avoid reflections or, more precisely, to make sure they're very low in comparison with the wanted signal. Reference [35], in which the ground impedance at low frequencies is measured with the phase gradient technique and a source height of 7 meters, gives some recommendations. For large and highly reflecting objects (buildings), in this case modelled as a semi-infinite plane, a distance of not less than 300 meters is proposed, equal to a ratio of direct sound pressure to reflection of approx. 40 dB. For smaller objects like persons or tree trunks, a minimum distance of 30 meters (approx. four times the maximum source-microphone distance) is recommended. Happily, smaller objects like the loudspeaker support made from angled steel did not have an influence on the results. Although, strictly speaking, these recommendations are valid only for the phase gradient method, it is evident that any reflecting object should be placed as far from the set-up as possible.

## IX. Absorber models

Models for predicting the characteristic impedance and wave number of materials play a twofold role in connecting with ground impedance measurements. On the one hand, they can be used to verify measurement results if absorber parameters for the ground under test – or a similar ground – are known from non-acoustic measurements or from the literature. However, acquiring parameters like flow resistivity, porosity and tortuosity is far from trivial for natural grounds as it requires multiple undisturbed sample to be taken. One may well ask if such an approach is reasonable because one could as well use these samples to measure the characteristic impedance and wave number directly, e.g. in a four microphone impedance tube [60].

On the other hand, acoustic measurements can be used to obtain estimates of the absorber parameters by matching the predicted excess attenuation, transfer function (“template method”) or effective impedance with the observed one.

The parameters derived from acoustical measurements will, in general, not agree with the values from non-acoustic measurements, especially if an absorber model with a low number of parameters is used. An example is the flow resistivity obtained by fitting to an one parameter absorber model. While some researchers [61] have found that the static flow resistivity is roughly twice as high as the acoustically derived one, others [62] observed the reverse situation. Obviously, parameters not taken into account have influenced the acoustical properties of the ground. The acoustically derived parameters are often called “effective” parameters. If a definition of an effective parameter is provided it is important to note that this definition will only be valid for the stated model.

In this chapter, selected absorber models having found suitable for grounds will be presented. A more elaborate overview can be found in [54] and [63]. The selection will be restricted to models which assume a fluid-like behaviour (rigid frame models). More sophisticated models which take into account structural vibrations (e.g. the Biot model [64]) will not be considered because they feature a large number of parameters which are rarely available (require uncommon procedures for their determination) and can't be deduced from simple acoustic measurements.

For deducting the effective surface impedance from the characteristic impedance and wave number the reader is referred to the previous chapter. In case of hard backed layers, the thickness of the layer is then an additional parameter.

### Delany- Bazley / Miki (One parameter)

The Delany- Bazley model [65] is marked by its simplicity, it requires only one parameter, the flow resistivity. This simplicity and the high age (published 1970) has made it the most famous and wide-spread model for porous absorbers. It is an empirical model originating from a regression analysis of the acoustical properties and the static air flow resistivity  $\sigma$  of fibrous absorbers with a high porosity (e.g. glass wool). The (normalised) characteristic impedance and wave number are given by eq.44 and 45.

$$Z_c = 1 + 9.08 \left( 10^3 \frac{f}{\sigma} \right)^{-0.75} + i 11.9 \left( 10^3 \frac{f}{\sigma} \right)^{-0.73} \quad (44)$$

$$k' = 1 + 10.08 \left( 10^3 \frac{f}{\sigma} \right)^{-0.70} + i 10.3 \left( 10^3 \frac{f}{\sigma} \right)^{-0.59} \quad (45)$$

For materials with a porosity  $\Omega$  smaller than one, agreement between predicted and measured impedance can be improved by using an effective flow resistivity of  $\sigma_{\text{eff}} = \sigma \Omega$  [54].

These equations are considered valid for  $0.01 < f/\sigma < 1$ ; this makes the use of these relationships for low frequencies and high flow resistivities commonly occurring in natural grounds questionable.

It has been observed that the Delany- Bazely model can sometimes predict non-physical results for low frequencies and layered media. Hence, an improved relationship, based on the same data, has been suggested (Miki model) [66]:

$$Z_c = 1 + 5.50 \left( 10^3 \frac{f}{\sigma} \right)^{-0.632} + i 8.43 \left( 10^3 \frac{f}{\sigma} \right)^{-0.632} \quad (46)$$

$$k' = 1 + 7.81 \left( 10^3 \frac{f}{\sigma} \right)^{-0.618} + i 11.41 \left( 10^3 \frac{f}{\sigma} \right)^{-0.618} \quad (47)$$

While nowadays the Miki expression should be preferred, the elapsed time of twenty years between the two models provokes a still extensive use of the original model as a lot of people have become accustomed to it. We will follow this custom in this work.

### Exponential changing porosity (Two / three parameters)

The Delany- Bazley model is limited in that the relationship between real and imaginary part of the impedance is fixed. Additionally, it assumes that the properties of the medium do not change with depth. In natural grounds, one can often expect a decrease of porosity with depth as the upper part is loosened by plant roots or cultivation while deeper sections are compacted due to the weight of the overlying sections as well as the sedimentation of finer particles. To account for this change of porosity, a two parameter model has been proposed [63]. The model ("2PA") assumes an exponential change of the porosity with depth (eq.51) and is a low frequency, high flow resistivity approximation.

$$Z_c = \frac{1}{\sqrt{\pi \gamma \rho_0}} \sqrt{\frac{\sigma_e}{f}} (1+i) + i \left( \frac{c_0 \alpha_e}{8 \pi \gamma f} \right) \quad (48)$$

$$k' = Z_c \cdot \gamma \Omega_0 \quad (49)$$

$$\sigma_e = \sigma \frac{s_p^2}{\Omega_0}, \quad \alpha_e = \frac{\alpha}{\Omega_0} \quad (50)$$

$$\Omega = \Omega_0 e^{-\alpha z} \quad (51)$$

with the effective flow resistivity  $\sigma_e$ , the effective rate of change of porosity  $\alpha_e$  and the ratio of specific heats in air  $\gamma$ ; porosity near the surface  $\Omega_0$ , pore shape factor  $s_p$  and depth  $z$ .

From equation 48 it can be seen that a positive value of  $\alpha_e$  – tantamount to a decrease of porosity with depth – gives an impedance with an imaginary part higher than the real part. This situation has some similarity to the hard backed case shown in fig.14. On the other hand, if the real part exceeds the imaginary part at low frequencies, this is an indication of a compacted / encrusted upper layer. As long as the wave number is not needed (semi-infinite case), the model has only two adjustable effective parameters while still providing a reasonable flexibility: "In particular, microstructurally based two-parameter models (2PA or NHBL2A) are recommended since they allow tolerable agreement between prediction and data for surface impedance of a wide variety of ground surfaces." [63]. The good performance has led to this model being recommended in ANSI S1.18.

### Micro-structural model (Three / four parameters)

By generalisation of the Rayleigh's model [67] of an absorber with a rigid frame and cylindrical, straight and parallel pores, an exact model ("H4A") for absorbers with arbitrary shaped pores can be derived [68]. Normalised wave number and characteristic impedance are given by eq.52 and 53.

$$k'^2 = q^2 \frac{1}{1 - 2(\lambda \sqrt{i})^{-1} T(\lambda \sqrt{i})} \left( 1 + 2(\gamma - 1) \frac{1}{\sqrt{N_{pr}} \lambda \sqrt{i}} T(\sqrt{N_{pr}} \lambda \sqrt{i}) \right) \quad (52)$$



$$Z_c = \frac{1}{Z_0} \frac{\omega}{k'k} \rho_b = \frac{1}{k'} \frac{q^2}{\Omega} \frac{1}{1 - 2(\lambda\sqrt{i})^{-1} T(\lambda\sqrt{i})} \quad (53)$$

with

$$\lambda = \frac{1}{s_p} \sqrt{\frac{2\rho_0 q^2 \omega}{\Omega \sigma}}, \quad T(x) = \frac{J_1(x)}{J_0(x)} \text{ and } q^2 = \Omega^{-n'} \quad (54)$$

the tortuosity  $q^2$ , the Prandtl number  $N_{pr}$ , grain shape factor  $n'$  and  $J_0/ J_1$  cylindrical Bessel functions of zeroth resp. first order. This model has four adjustable parameters. For small values of  $\lambda$ , corresponding to low frequency and/ or high flow resistivity, the following approximation is possible ("H3A") [54]:

$$k'^2 = \gamma \left( \left( \frac{4}{3} - \frac{\gamma-1}{\gamma} N_{pr} \right) q^2 + i \frac{4s_p^2 \sigma \Omega}{\omega \rho_0} \right) \quad (55)$$

$$Z_c = \frac{1}{k'} \left( \frac{4q^2}{3\Omega} + i \frac{4s_p^2 \sigma}{\omega \rho_0} \right) \quad (56)$$

By defining an effective flow resistivity of  $\sigma_e = \sigma (s_p^2 / \Omega)$  or  $\sigma_{pe} = \sigma (s_p^2 \Omega)$ , a three parameter model is obtained.

For very high flow resistivities or low frequencies, eq.55 and 56 simplify to eq.48 and 49 with  $\alpha = 0$  ("H1A").

In figure 20, the "exact" four parameter model (eq.54), the three parameter (eq.56), the one parameter approximation (eq.48,  $\alpha=0$ ), the Miki (eq.46) and the Delany-Bazely (eq.44) model are compared for a material with a flow resistivity of 100 krayl/m and a porosity of 0.4. The three parameter model is practically identical to the exact model, only for grounds with very low flow resistivity, and high frequencies, the four parameter model may be needed. The Delany-Bazely model, on the other hand, does not agree with the exact model for most frequencies; the Miki model shows a better agreement, especially in the real part. The one parameter approximation shows increasing deviations with rising frequency and becomes similar to the Miki and DB model. However, the two parameter model (derived from the one parameter approximation) may still be the best choice if one is interested in smoothing or extrapolation of impedance data (for not too high frequencies). While in some situations the gained absorber parameters may loose their physical meaning [63], the 2PA model does still offer a good fit to the data. More important, for any single measurement of the impedance, the two parameters of the model will be unique. This is not the case when trying to fit the three parameter model, because "for any geometry configuration, there could be two different combinations of effective flow resistivity  $\rho_{pe}$ , tortuosity  $T$ , and porosity  $\Omega$  giving the same or similar rms values" [69] (of the least square fit to a level difference spectrum). To resolve this indeterminacy, either one of the parameters (e.g. porosity) has to be measured independently or one measures the wave number in the ground with a pair of buried microphones [70].

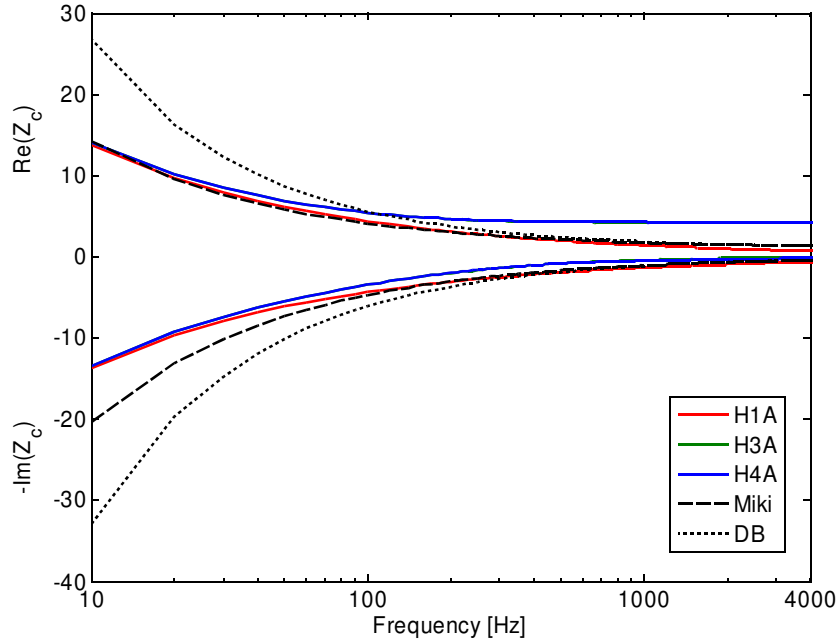


Figure 20: Comparison of the characteristic impedance  $Z_c$  predicted by the four parameter model (H4A), the three parameter (H3A), the one parameter (H1A) approximation, the Miki and the Delany-Bazley model.  $\sigma = 100 \text{ krayl/m}$ ,  $\Omega = 0.4$ ,  $n = 1$  and  $s_p = 0.2$ .

## Overview of absorber parameters of grounds

For verification of own measurement results as well as for theoretical studies it is helpful to have an overview of absorber parameters of common outdoor materials. Data by several authors has been compiled and are presented in the tables 3 - 5, grouped by absorber model.

The most important parameter, the effective flow resistivity  $\sigma_e$ , features a large range from near 1 krayl/m for snow to more than 1,000 krayl/m for wet and compacted grounds. It is worth noting that even for apparently identical grounds, like institutional grass, the absorber parameters can vary significantly. The condition of the ground (dry/wet, loose,/compacted, cultivated or not) will likewise have an influence on its acoustical properties.

Data for porous asphalt (tab.5) has been included to demonstrate that, apart from snow, this is one of the few materials where extended reaction (thin layers of low flow resistivity above hard backing) becomes important.

Finally, the absorber parameters deduced from acoustical measurements will depend on the chosen absorber model and special attention has to be given to the definition the respected author has used for the "effective" parameters. Unfortunately, the definition may not only depend on the author but the same author may use differing definitions in his or her publications. The same problem exists for the shape factors which came in the flavours  $s_p$  (pore shape factor),  $s_f$  (shape factor ratio,  $n'$  (grain shape factor) and  $s$  (static shape factor). The relation  $s_f = n'/\sqrt{s} = 2s_p$  will prove helpful for conversion.

Ground	Layer/ condition	Model	Direct		Acoustical			Ref.
			$\sigma$	$\Omega$	$\sigma_e^{**}$	$\Omega$	T	
Snow*	Low $\sigma_e$	H4A	8.9	0.77	2.1	0.76	1.3	71
Snow*	Medium $\sigma_e$	H4A	13.4	0.68	4.1	0.67	1.3	71
Snow*	High $\sigma_e$	H4A	14.0	0.62	5.0	0.59	1.4	64
Deep snow		H3A			4.5	0.88	2.7	63
New snow		H3A			5.5	0.64	1.5	63
Crusted snow		H3A			30.0	0.5	4.0	63
Snow		H3A		0.52 –0.60	3.9	0.6	1.1	69
Snow		H3A		0.73 –0.76	4.5	0.88	2.7	69
Clay	Unwheeled	H3A		0.55	19.3	0.57	3.4	69
Clay	Wheeled	H3A		0.47	20.9	0.42	2.7	69
Silt	Cultivated	H3A		0.54	27.6	0.56	2.9	69
Sandy loam	Moist	H3A		0.33	61.7	0.39	1.2	69
Sand		H3A		0.47	82.7	0.48	1.3	69
Sandy loam	Dry	H3A		0.49	88.9	0.52	3.3	69
Sand		H3A		0.35	324	0.36	2.2	69
Silt	Compacted	H3A		0.23	440	0.18	2.4	69
Catalpa silty clay loam*	Intermediate, loose	H3A			33.4	0.4	2.9	72
Catalpa silty clay loam*	Intermediate, compacted	H3A		0.26	40.7	0.3	2.3	72
Masonry sand*	Intermediate, loose	H3A		0.46	41.7	0.38	1.4	72
Masonry sand*	Dry, loose	H3A		0.45	83.0	0.42	2.8	72
Masonry sand*	Dry, compacted	H3A		0.41	112	0.42	2.5	72
Masonry sand*	Intermediate, compacted	H3A		0.37	161	0.41	2.4	72
Catalpa silty clay loam*	Dry, compacted	H3A		0.45	226	0.42	3.5	72
Catalpa silty clay loam*	Dry, loose	H3A		0.45	244	0.41	1.7	72
Grenada silt loam*	Dry, compacted	H3A		0.49	914	0.46	10.9	72
Grenada silt loam*	Intermediate, loose	H3A		0.37	968	0.37	4.8	72
Grenada silt loam*	Wet, compacted	H3A		0.27	1598	0.23	15.5	72
Catalpa silty clay loam*	Wet, compacted	H3A		0.28	2189	0.25	14.6	72

Table 3: Overview of absorber parameters of natural grounds obtained by direct measurement or fit of acoustical data to the H4A and H3A model. Flow resistivities in krayl/m. \*: Averaged data. \*\*:  $\sigma_e = \sigma (s_p^2 / \Omega)$ .

Ground	Layer/ condition	Model	Direct	Acoustical		Ref.
			$\Omega$	$\sigma_e / \sigma_{eff}$	$\alpha_e$	
Powdered snow	Over frozen ground	2PA		3.5	3	63
Pine forest		2PA		7.5	25	63
Institutional grass		2PA		30	250	63
Grassy lawn		2PA		35	30	63
Loose earth		2PA		50	80	63
Meadow		2PA		57	95	63
Hard worn lawn		2PA		75	120	63
Compacted earth	Dry	2PA?		140	10	63
Institutional grass		2PA		140	35	63
Partly grass-covered		2PA		630	188	63
Grass covered field		H1A		95		63
Sandy soil		H1A		365		63
Snow	Dry, over older snow	DB		10 – 30		61
Sugar snow		DB		25 – 50		61
Forest, pine or hemlock		DB		20 – 80		61
Grass, rough pasture		DB		150 – 300		61
Roadside dirt	With small rocks	DB		300 – 800		61
Sandy silt	Hard packed	DB		800 – 2500		61
Limestone chips	1 – 2,5 cm	DB		1500 – 4000		61
Dirt roadway	Old, interstices filled	DB		2000 – 4000		61
Earth	Rain packed	DB		4000 – 8000		61
Quarry dust	Very hard packed	DB		5000 – 20000		61
Asphalt	Sealed	DB		30000		61
Beech forest		DB	0.46	34.5		73
Forest, mixed deciduous	Without Litter, humus	DB		52.8		73
Forest, mixed deciduous		DB		53.8		73
Forest, mixed deciduous	Without litter	DB		60.2		73
Beech forest	Without litter	DB	0.46?	69.9		73
Forest, mixed deciduous		DB	0.45	118		73
Forest, fir	Without litter	DB	0.61?	121		73
Grass		DB	0.5	174		73
Meadow		DB	0.57	204		73
Loamy sand		DB	0.43	1410		73
Loamy sand		DB	0.47	2137		73

Table 4: Overview of absorber parameters of natural grounds obtained by direct measurement or fit of acoustical data to the 2PA, H1A and Delany-Bazley model. Flow resistivities in krayl/m. ?: Missing / uncertain data.

Ground	Layer thickness	Model	Direct		Acoustical	Ref.
			$\sigma$	$\Omega$	T	
Porous asphalt	4 cm	Other	2	0.3	3.3	74
Porous asphalt	4 cm	Other	5	0.15	2.5	74
Porous asphalt	4 cm	Other	15	0.15	3.3	74
Porous asphalt	2.5 cm	Other	15	0.15	2	74

*Table 5: Absorber parameters of porous asphalt from direct and acoustical measurements. Flow resistivities in krayl/m.*

## X. Effect of ground condition

The impedance of a specific ground is not a constant, even if one surveys a fixed location. It will vary with the state of the ground, which changes with time, weather conditions and due to external intervention. Table 3 already demonstrates that the degree of compaction and the water content influence the effective flow resistivity and hence the impedance. As the water saturation is a parameter which is subject to rapid and extensive variations its influence will now be discussed in detail.

### Water saturation

The effect of a change in moisture content on grassland and barren earth has been studied by [75], the ground impedance was deduced from excess attenuation measurements with a source-microphone distance of 4 m. The dry ground with a moisture content of 10 % and an effective flow resistivity  $\sigma_{\text{eff}} = 200$  krayl/m showed an almost monotonous decrease of the impedance with frequency, which did not vary much depending on the location. After irrigation of the area to attain a moisture content of 35 %, the impedance increased substantially, but measurements at different locations showed little consistency. Some measurements showed a maximum in the impedance near 700 Hz, others a continuous increase for frequencies lower than 2 kHz. In all cases, narrow resonances were found in the 3 to 9 kHz region. Barren earth ( $\sigma_{\text{eff}} = 200$  krayl/m), first dug up 40 cm deep and then raked flat, showed a similar behaviour when changing the water content from 10 to 32 %. However, if the earth was broken up and redigged after the irrigation, almost no change in the impedance was observed. These measurements demonstrate that an increased moisture content does not simply lead to an increased impedance, a relation one could anticipate because added water will decrease the porosity as it fills the pores and produces swelling in some minerals leading to an increased effective flow resistivity. Water can also lead to coagulation of soil particles leading, under certain circumstances, to layering of the ground subsequently resulting in local maxima (resonances) in the surface impedance. Laboratory studies by [76] based on impedance measurements on sand in a two microphone tube partly confirm these results. Coarse sand ( $\sigma = 85$  krayl/m,  $\Omega = 0.39 \rightarrow \sigma_{\text{eff}} = 33.2$  krayl/m) displayed a maximum in the imaginary part of the admittance near 500 Hz due to the secondary reflection on the water table (extended reaction, hard-backed layer). Fine silica sand ( $\sigma = 314$  krayl/m,  $\Omega = 0.44 \rightarrow \sigma_{\text{eff}} = 138.2$  krayl/m), on the other hand, did not demonstrate extended reaction but showed a continuous increase in impedance with increasing water saturation. For both sands, the change in admittance was the highest for a change of the water saturation from 0 % (dry) to 10 %, whereas changes above 76 % had a much lesser effect.

Already these selected investigations demonstrate that the ground impedance is a parameter subject to substantial fluctuations. Not only can apparently identical grounds have widely varying impedances, but also the impedance of a specific ground may vary significantly due to changes in its state, e.g. due to changing moisture content. In addition, hardly any (in-situ) studies exist which would allow an assessment of the real variability of the ground impedance of natural grounds.

## **XI. Published results**

It is about time to present the integral results of this work. The fundamentals have been thoroughly outlined: the sound field model, its assumptions and used approximations have been presented. The absorber models in combination with data from the literature (tables 3 - 4) are suggestive of which course of ground impedance one has to expect and which properties of the ground follow hereof. In addition, the effects of external influences must be kept in mind when choosing the measurement conditions.

Most important is, however, the overview of available in-situ impedance (or reflection coefficient) measurement methods, as it permitted a preselection of procedures which may be especially fit for the determination of ground impedances in the lower frequency range, below approx. 1 kHz. By having regard to already known examples of the performance of specific methods and by observing their ease of use, the two-microphone transfer function method has been chosen for a closer investigation.

For this purpose, a three-step proceeding has been used.

First, measurements were done on different grounds with the three geometries suggested by ANSI S1.18 (template method) to test if the performance of the method depends on the ground impedance or geometry. During these test, it was also checked how good the repeatability of the two-microphone method is and which variability of the impedance inside an apparently homogeneous area has to be expect.

The results were published in:

### **Acta Acustica: Application of the two-microphone method for in-situ ground impedance measurements (P1)**

Second, the causes for the deviations of the measurement results from the expectations were analysed. This time, a numerical simulation was used to investigate the influence of unavoidable measurement uncertainties on the deduced surface impedance. As a consequence, a first optimisation of the method is proposed, the use of geometries particularly suit for the low frequency range from 100 – 400 Hz:

### **Applied Acoustics: Effect and minimization of errors in in-situ ground impedance measurements (P2)**

The third step was to look for alternatives to a changed geometry in order to improves the performance of the transfer function method at low frequencies. Procedures routinely used for impedance tube measurements were applied to the in-situ technique to check if they are beneficial even in outdoor situations:

### **Acta Acustica: Reducing the influence of microphone errors on in- situ ground impedance measurements (P3)**

The investigations were not strictly limited to the two-microphone method. A second examined method was the use of a microflown/microphone combination to obtain the field impedance which was subsequently used for sound field matching. Because of the scarce advance informations available – due to the microflown being a rather new device hardly used for such types of measurements – it was decided to do a study under controlled laboratory conditions with well-known materials to check what results can be expected from this approach:

### **JASA: Measuring the free field acoustic impedance and absorption coefficient of sound absorbing materials with a combined particle velocity - pressure sensor (P4)**

All four publications can be found at the end of this thesis.





## XII. Summary and conclusion

The already published results from the previous chapter shall now be summarised to gain an overall picture of the effectiveness of the two-microphone technique and to demonstrate the attained improvements. Albeit most results have already been presented, it will be resorted to additional measurement results to clarify other relevant interrelations.

### The standard ANSI S1.18 procedure

The initial measurements with the geometries suggested by ANSI S1.18 already demonstrate the general adequacy of the transfer function method for the direct deduction of ground impedances. For not too hard grounds, believable results were sustained for frequencies above approximately 300 Hz, in agreement with data from the literature. The procedure exhibited a good repeatability, only minor variations were observed if the measurement was repeated at the same location. The variability of the estimated impedance within the area of investigation was significantly higher, reminding the user that dependable estimates can only be expected if an average of a number of locations was used. In this context, it was noted that it is sometimes better to first average the transfer functions in comparison with averaging the impedance estimates.

The found differences between the three geometries were insightful: while geometry A and B (table 1) led to similar results, geometry C (which is only recommended for soft grounds) did not show a good performance in any of the investigated situations. This suggested that it is promising to have a closer look at the geometry dependence of the method's performance.

After the initial measurements, two problems have been identified: the poor performance in the low frequency range (below about 300 – 400 Hz) and the poor performance for hard grounds.

### Analysis of the problem

It was necessary to have a closer look at the reasons for the insufficient low frequency performance to get to the root of the problem. As mentioned in chapter IV, the level difference below approx. 400 Hz will not depend much on the flow resistivity of the ground or, in other words, on its impedance. Conversely, this means that minor errors in the level difference lead to sizeable errors in the deduced surface impedance. Such errors can hardly be avoided, especially keeping in mind that we are dealing with outdoor measurements and not a tightly controlled laboratory environment. The situation is thoroughly investigated in publication P2. The accuracy of the level difference is major factor, even errors in the range of the precision of typical measurement equipment are sufficient to generate the observed deviations of the observed impedance from the anticipated one. To a lesser degree (for the investigated geometry), errors in the geometry – which in light of a natural ground not really being a well-defined plane have to be anticipated - can lead to errors in the deduced impedance.

The relation between errors in the transfer function and the resulting impedance error has a troublesome property: it is neither linear nor symmetric in the sense that a certain error in the level difference (e.g. + 0.2 dB) will lead to an error similar in size, but opposite in direction compared to the opposite error (e.g. -0.2 dB). This explains why there are differences in the deduced impedance if one first averages several measurements and then calculates the impedance versus averaging the single impedances. This also means that even if the errors had a zero mean distribution one would only obtain the correct result if one averages the transfer functions first. The effect of errors in the geometry is, fortunately, largely symmetric so that one can hope it averages out unless there are constant errors in the geometry.

The degree of the impact of measurement uncertainties on the impedance estimate does also depend on the surface impedance, with high impedance surfaces being more critical than low impedance ones.

The results of the numerical simulation in publication P2 agree well with the experimental results from publication P1.

The question is now how to improve the two-microphone method for a better performance below about 400 Hz. As long as one wants to keep the basic principle of the method, one must either make the procedure more error prone or must reduce the errors in the transfer function.

## Optimised geometry

To make the method more robust, one must bear in mind that the effect of errors will depend, for any given combination of ground impedance and frequency, on the measurement geometry. Thus, for a chosen frequency range and having an estimate of the surface impedance as well as estimates of the measurement accuracy, an optimisation is possible to find the geometry that is least sensitive to the errors.

The results of the optimisation are promising, with an expected decrease in the average error in the impedance of 50 % compared to the three geometries from the ANSI standard. In the publication, only an example for single bounds of the geometry is given. However, one can observe the following trends: The source- receiver distance will be at the upper limit, the lower microphone height at the lower limit and the upper microphone height near the upper limit; the optimal source height will be near the midpoint between upper and lower microphone.

The course of action chosen in P2 may appear crude, but the highly non-linear interrelation between transfer function and impedance did leave no other choice when to use the "simulated empirical variances": with the first order derivative being no good approximation of the actual function, it was not possible to rely on the Gaussian error propagation law to obtain an estimate of the total error, even though calculation of the derivatives is straightforward and the calculation would be much faster. In addition, it was not possible to solely concentrate on errors in the level difference and neglect errors in the geometry as both factors are not independent. A geometry largely insensitive to level difference uncertainties can be very sensitive to an imprecise geometry.

## Reducing the influence of microphone errors

In order to reduce the errors in the transfer function – in contrast to reducing their effect by use of an adapted geometry – it must be recalled what the sources of the errors in the level difference are. On the one hand, there are random factors like unwanted reflections, fluctuating propagation conditions and background noise. On the other hand, there are (more or less) constant factors like differences in the sensitivities of the microphones and the input channels of the analyser. These constant errors can't be reduced by repeated measurements and hence were of special interest. While no differences between the inputs of the analyser could be found, one has to expect marginal differences in the frequency responses of the two microphones even though they were of high quality and the same type. These differences in sensitivity also interfere with the transfer function method for measuring the impedance in an impedance tube [6], so that solutions are readily available: either one measures with one microphone successively in two positions [77] or, more common, does two measurements with the microphones in "normal" and "switched" position [78]. Both procedure are expected to eliminate the differences resulting from imperfections of the equipment as long as the sound field is stationary. While the situation is simple in an impedance tube, the actual improvement by using one of the mentioned methods in an outdoor situation can hardly be predicted. The difference in the microphones' sensitivities may account only for a small part of the error in the transfer function. Furthermore, the assumption of stationarity is questionable. The results, however, clearly show that at least the switched microphone technique leads to significantly improved impedance estimates below approx. 500 Hz, whereas the one-microphone switched position technique suffers from the sound field instationarity and can only be recommended for especially favourable conditions (low source-microphone distance, wind speed and background noise).

## Additional sources of errors: The sound source

The microphones are not the only part of the equipment which influence the low frequency performance of the two-microphone method. While there are hardly any indications in the literature for explaining poor low frequency results, in [31] the authors observe such problems and assumes that the sound pressure may simply be too low, possible because of following the recommendation of ANSI S1.18 to use a "compression driver plus pipe" type of source which can be regarded as a good analogue to a point source. Unfortunately, this type of source will regularly not have a reasonably high power in the low frequency range, so that its use for higher source-receiver distances or in case of non-negligible background noise is questionable.

An example for source related problems is given in fig.21. The ground impedance of a compacted, dry lawn was measured with a large geometry (see figure caption) and two different sound sources: a broadband speaker with 10 cm diameter and a 25 cm woofer, both in a closed box.

Although the sound pressure of the pink noise was comparable at the microphones' positions (80 – 85 dB(A)), the results only agree above 150 Hz. Below, the sound power of the small loudspeaker was obviously not sufficient and the impedance estimate is implausible, even though the sound pressure between 100 and 150 Hz was not so low that the transfer function between the microphone signals become random, as the observed coherency was near unity.

Thus, it is required that the sound pressure be well above the background noise, at least for low frequencies, so that the transfer function is solely determined by the sound originating from the loudspeaker and not influenced by background noise.

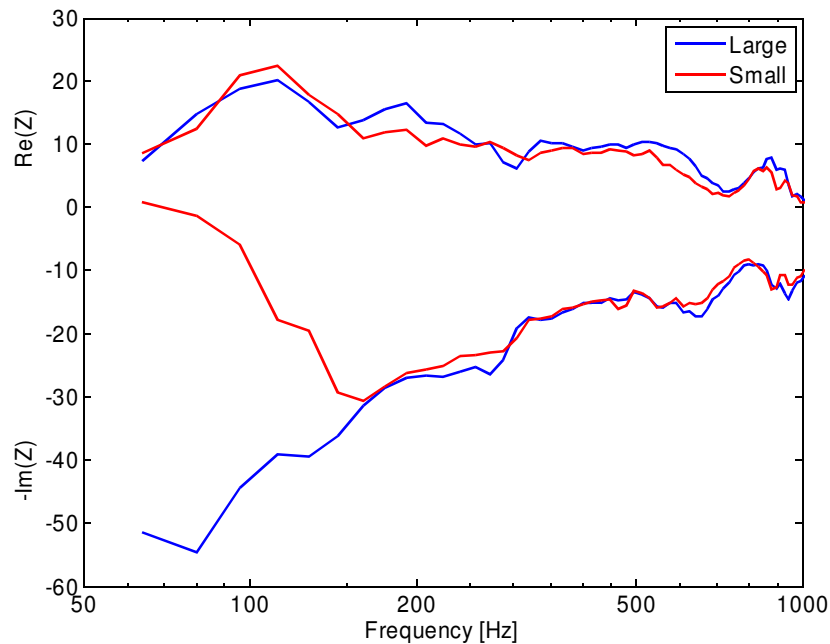


Figure 21: Ground impedance of a compacted, dry lawn. Comparison of results obtained with small loudspeaker (10 cm) and large woofer (25 cm). Geometry:  $h_s = 0.8$  m,  $h_{ru} = 1$  m,  $h_{rl} = 5$  cm and  $R = 5$  m.

## Experimental verification, combination of optimised geometry and switched microphone technique

What is missing, at this point, is the experimental verification of the simulation results from publication P2, the optimised geometry. Furthermore, the combination of an optimised geometry with the switched microphones technique shall be investigated.

For that purpose, three examples shall be given which originate from measurements above dry sand. Measurements were done with geometry A (fig.22) and two optimised geometries, one from publication P2 (fig.23) and a larger geometry (fig.24) which should have an even higher error tolerance [79].

These examples clearly show the advantages of both the optimised geometries and the switched microphones technique. The measurements with the non-optimised geometry A (fig.22) demonstrate that no reasonable impedance estimate below approx. 250 Hz could be obtained with the microphones in either "normal" or "switched" position. What is especially remarkable is the large difference between the measurements which should not occur if the equipment was faultless. With the mean/corrected transfer function calculated from both measurements, on the other hand, the impedance estimate increases with decreasing frequency down to 80 Hz, as acoustically expected for a rigid-porous absorber.

The situation is partly different for the measurements with the optimised geometries (fig. 23 and 24). In this case, the deduced impedance shows a continuous decrease with increasing frequency from 100 to 600 Hz (admittedly, some smoothing would be appropriate), even if the microphones were only used in "normal" or "switched" positions. Using the mean transfer function did not lead to an improvement because the geometry is already largely tolerant to errors in the transfer function.

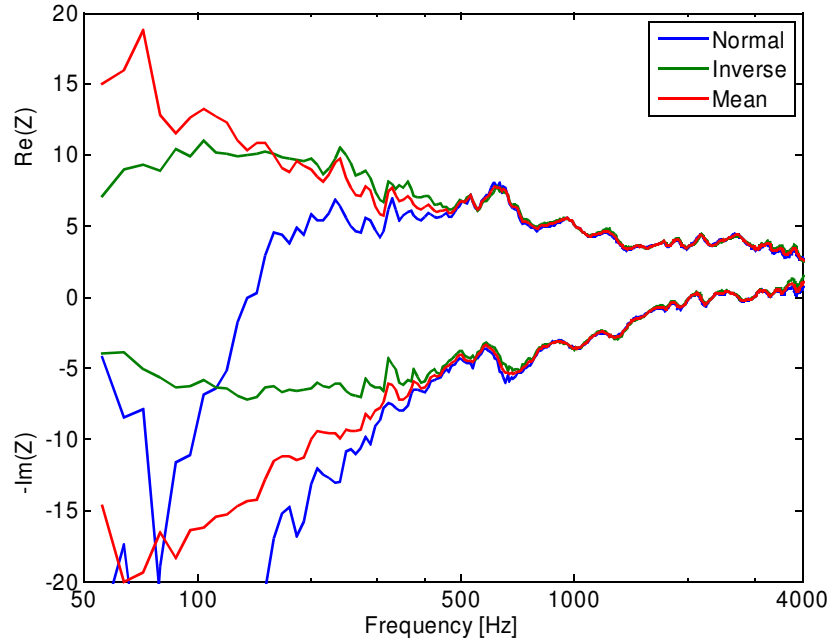


Figure 22: Impedance of sand measured with geometry A from ANSI S1.18. Switched microphones technique: microphones in “normal” position (Normal), microphones’ positions switched (Inverse) and corrected/ mean transfer function from both measurements (Mean).

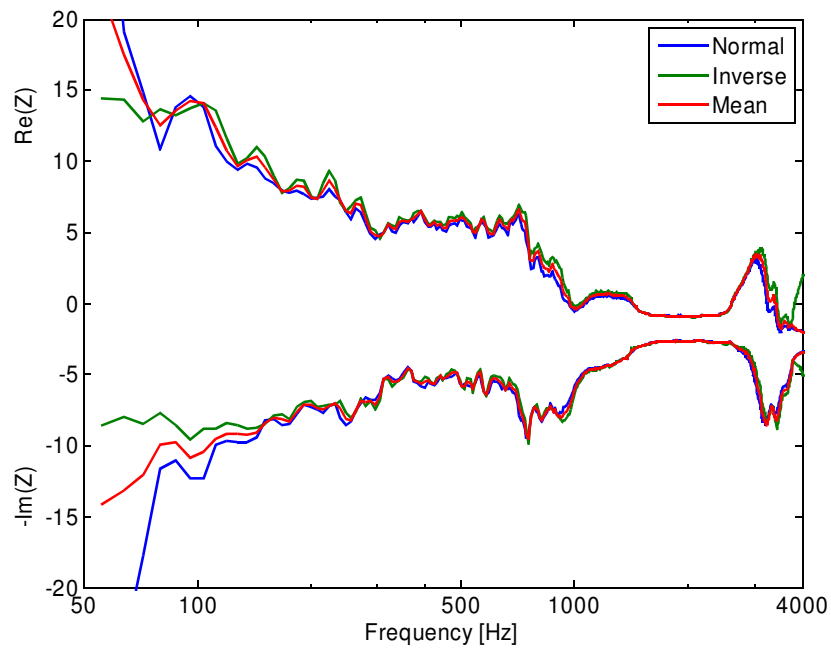


Figure 23: Impedance of sand measured with the optimised geometry from publication P2.  $h_s = 0.5$  m,  $h_{ru} = 0.95$  m,  $h_r = 5$  cm and  $R = 3$  m. Switched microphones technique.

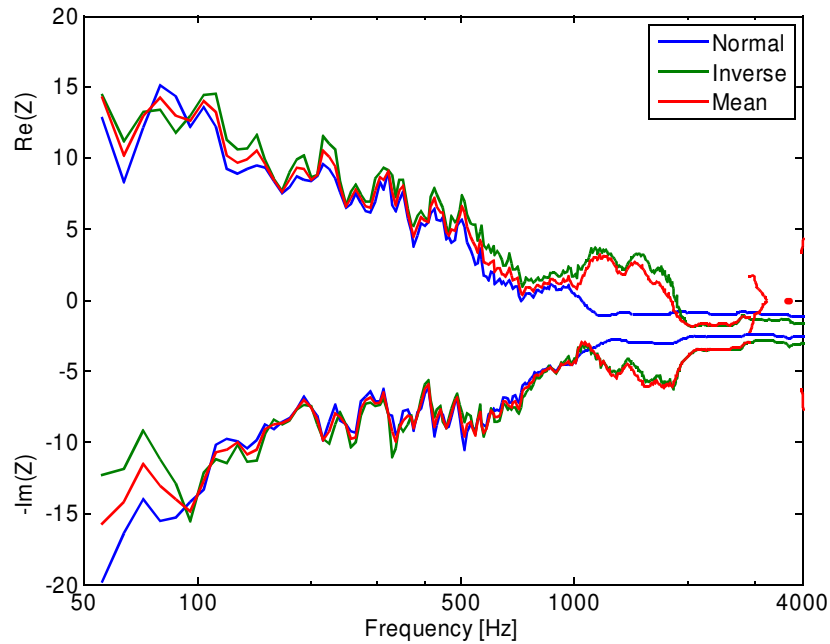


Figure 24: Impedance of sand measured with a large optimised geometry.  $h_s = 0.8$  m,  $h_{ru} = 1.3$  m,  $h_{rl} = 5$  cm and  $R = 5$  m. Switched microphones technique.

The results above 600 Hz are not inspiring confidence, but it must be remembered that the geometries were optimised for the frequency range 100 – 400 Hz: above 400 Hz, the two geometries may well be more sensitive to measurement uncertainties (in the geometry) than the “standard” geometries. Hence, it is advisable to measure with more than one geometry – a large one optimised for low frequencies and a smaller one (like geometry B) for higher frequencies – to obtain impedance estimates over the entire frequency range of interest. This course of action will also be suggested in the upcoming successor of ANSI S1.18 [4].

All in all, the suggested improvements, switched microphones, optimised geometry and large loudspeaker, lead to a significantly higher accuracy of the deduced impedance below approx. 500 Hz with hardly any additional effort. Consequently, the two-microphone transfer function technique can be considered to be the method of choice for in-situ ground impedance measurements for frequencies above 100 Hz, with further improvements still possible.

### Microflown based measurements

What remains are the results of using a microflown/ microphone combination (“PU probe”) for sound field matching. In this case, two major conclusions can be drawn: on the one hand, by using the “correct” sound field model (eq.21), impedance estimates agreeing reasonably well with the predictions of an absorber model for frequencies larger than 300 Hz could be obtained, in contrast to assuming a plane wave like reflection as common before. On the other hand, improper calibration of the microflown can severely degrade the low frequency performance of the method, only the calibration in a Kundt's tube has been found to be acceptable.

In general, it remains questionable if, for the purpose of surface impedance deduction, using a PU probe does have any advantage compared to using a pair of microphones.



### **XIII. Outlook**

The results of this work are, first and foremost, improvements to the existing two-microphone method for in-situ impedance measurements. Because of their demonstrated effectiveness and ease of use, an optimised geometry as well as the switched microphones technique are under consideration to be included in the successor of ANSI S1.18 [4].

In the long run, what may be of even greater benefit for future perfection of the method is the finding what the reasons for the often observed errors in the deduced surface impedance are: the inaccuracy of the transfer function and the geometry.

#### **A global optimisation including external influences**

The key to further refinements are proper estimates of the measurement uncertainties. The numbers for the geometry optimisation were simplified: they depended neither on the frequency nor on the geometry itself. This is not very realistic: the geometry can typically be determined with a certain relative accuracy, e.g. one percent. It must also be foreseen that the uncertainty of the transfer function increases with increasing distance between source and microphones and with increasing microphone separation due to atmospheric effects (turbulence, wind profile, thermal stratification) and the amplified influence of unwanted reflections. If these factors can be quantified an even better optimised geometry will be found allowing impedance measurements at frequencies below 100 Hz: currently, with the constant error assumptions, the optimisation procedure tends to select the highest possible source-receiver distance and a large microphone separation, although there may actually be an optimal balance between error tolerance and increasing error size.

The optimisation should also include one source of errors not previously included: it was always assumed that the microphones were placed exactly one above the other (or, in other words, that the slant distance between source and receivers was equal). Although the placement of the microphones can be (and has been) checked with a water-level, a certain degree of tolerance towards this error would be preferable as it has been observed that it's effect can be rather high for low frequencies.

#### **The measurement equipment**

There are additional questions concerning the measurement accuracy, especially in relation to the "equality" of the microphones. The suggested switched microphones technique requires that two measurements are done at each location, but it would be more convenient if only one measurement was needed. It is possible that by using a phase matched pair of microphones (intensity probe), the error in the transfer function could be reduced satisfactory. Another possibility is to determine the difference between two conventional microphones one time in the laboratory and to use the result to subsequently correct the field data. Methods that cross one's mind are intensity calibrators, switched microphone calibration in an impedance tube and placing the microphones next to each other in a free field / anechoic room. Problematically, the required precision is quiet high, and one has to question if the laboratory data is still valid under outdoor conditions with different environmental temperature and humidity – the question of long term stability.

An approach to obtain better impedance estimates could also be to use more than two microphones. In that case, one has not only a single transfer function that is matched to the one predicted by the model but a whole set of transfer functions and it is possible that errors in the transfer function and geometry partially average out. The procedure would have some similarity to the phase gradient method [34].

#### **Optimising microflown based sound field matching**

On the other hand, it may be worth to give the microflown a second chance. The results from the laboratory tests were not very convincing, but one has to bear in mind that the procedure, unlike the two-microphone method, has not experienced nearly the same degree of fine-tune. This does not only concern the geometry (the microflown has another degree of freedom: it's orientation) but also it's calibration. It's unclear what accuracy one can achieve with the different calibration methods – by now, there are more than the two methods presented in publication P4.

Hence, it is still possible that a microflown / microphone combination can achieve the same or a better performance compared to the transfer function method, especially when thinking of high impedance surfaces.

What is problematic is the lacking experience regarding the deployment of microflows outdoors, they may be more affected by wind as it may overload them.

## General concerns

Finally, there are two basic questions independent of the measurement principle.

First, how representative are the deduced impedances, even if they were perfectly measured? It is clear that they are much better than impedance tube data or values from a table ("this is a lawn, it always has a flow resistivity of 125 krayl/m, so I can use model X and have an impedance...").

However, the properties of a ground change with weather condition and time. It would be advantageous if one had an estimate of the extent of the (seasonal) variability or even a model including, let's say, water saturation, temperature and "degree" of cover of vegetation. Unfortunately, data for that purpose is not available.

Second, how precise does the surface impedance need to be? Well, this depends on the intended application, and this will often be to predict noise level which residents are exposed to due to selected sound sources. It will be necessary to have a number of model cases for different source spectra, geometries and meteorological conditions to ascertain the situations – by numerical simulation - in which the ground has a significant influence. Only from the results of this simulation the needed precision of the ground impedance can be deduced and guidelines be provided regarding which situations require a high measurement accuracy and which do not.



## XIV. References

- 1 ISO 89613-2 (1999). "Attenuation of sound during propagation outdoors - Part 2: General method of calculation." International Organization for Standardization.
- 2 <http://www.imagine-project.org/>
- 3 Salomons, E. M. (2001). "Computational atmospheric acoustics." Kluwer Academic Publishers.
- 4 ANSI S1.18 draft (2008). "Method for Determining Ground Impedance." Acoustical Society of America.
- 5 ISO 10534-1 (1996). "Determination of sound absorption coefficient and impedance in impedance tubes - Part 1: Method using standing wave ratio." International Organization for Standardization.
- 6 ISO 10534-2 (1998). "Determination of sound absorption coefficient and impedance in impedance tubes - Part 2: Transfer-function method." International Organization for Standardization.
- 7 Jones, M. G. and P. E. Stiede (1997). "Comparison of methods for determining specific acoustic impedance." Journal of the Acoustical Society of America **101**(5): 2694-2704.
- 8 Jones, M. H. and T. L. Parrott (1989). "Evaluation of a multi-point method for determining acoustic impedance." Mechanical Systems and Signal Processing **3**(1): 15-35.
- 9 ISO 354 (2003). "Measurement of sound absorption in a reverberation room." International Organization for Standardization.
- 10 DEGA- Projekt (2004). "Akustische Wellen und Felder". Deutsche Gesellschaft für Akustik.
- 11 Kuhl, W. (1983). "Ursachen und Verhinderung systematischer Abweichungen vom "wahren" Absorptionsgrad bei der Absorptionsgradmessung im Hallraum." Acustica **52**(4): 197-210.
- 12 Dickinson, P. J. (1970). "Measurement of the normal acoustic impedance of ground surfaces." Journal of Sound and Vibration **13**(3): 309-323.
- 13 Tamura, M. (1990). "Spatial Fourier transform method of measuring reflection coefficients at oblique incidence. I: Theory and numerical examples." Journal of the Acoustical Society of America **88**(5): 2269-2264.
- 14 Tamura, M. (1995). "Spatial Fourier transform method of measuring reflection coefficients at oblique incidence.II: Experimental results." Journal of the Acoustical Society of America **97**(4): 2255-2262.
- 15 ISO 13472-1 (2002). "Measurement of sound absorption properties of road surfaces in situ - Part 1: Extended surface method." International Organization for Standardization.
- 16 CEN/TS 1793-5 (2003). "Road traffic noise reducing devices - Test method for determining the acoustic performance - Intrinsic characteristics - In situ values of sound reflection and airborne sound insulation."
- 17 Don, G. and A. J. Cramond (1985). "Soil impedance measurements by an acoustic pulse technique." Journal of the Acoustical Society of America **77**(4): 1601-1609.
- 18 Garai, M. (1993). "Measurement of the sound-absorption coefficient in situ: the reflexion method using pseudo-random sequences of maximum length." Applied Acoustics **39**(1/2): 119-139.
- 19 Wilms, U. and R. Heinz (1991). "In-situ Messung komplexer Reflexionsfaktoren von Wandflächen." Acustica **75**(1): 28-39.
- 20 Mommertz, E. (1995). "Angle-dependent in-situ measurements of reflection coefficients using a subtraction technique." Applied Acoustics **46**(3): 251-263.
- 21 <http://acustica.ing.unibo.it/Researches/barriers/adrienne.html>
- 22 Pazos, D., L. Weber, et al. (2006). Schallabsorption von Lärmschutzwänden: Vergleich unterschiedlicher Messverfahren. IBP-Mitteilungen, Fraunhofer Institut für Bauphysik.
- 23 Fuhs, S., R. Höldrich, et al. (2006). Validierung des Entfernungsgesetzes und Korrektur der Gruppenlaufzeit und des akustischen Zentrums des Lautsprechers im Adrienne-Verfahren. DAGA, Braunschweig.
- 24 Fuhs, S., R. Höldrich, et al. (2006). Korrektur der Lautsprecherrichtcharakteristik im Adrienne-Verfahren. DAGA, Braunschweig.
- 25 Bérengier, M. and M. Garai (2001). A state-of-the-art of in situ measurement of the sound absorption coefficient of road pavements. ICA, Rome.
- 26 ANSI S1.18 (1999). "Template method for ground impedance." Acoustical Society of America.
- 27 Allard, J. F. and Y. Champoux (1989). "In situ two-microphone technique for the measurement of the acoustic surface impedance of materials." Noise Contr. Eng. Journ. **32**(1): 15-23.
- 28 Allard, J. F., Y. Champoux, et al. (1989). "Pressure variation above a layer of absorbing material and impedance measurement at oblique incidence and low frequencies." Journal of the Acoustical Society of America **86**(2): 766-770.

- 29 Takahashi, Y., T. Otsuru, et al. (2003). "In situ measurements of absorption characteristics using two microphones and environmental "anonymous" noise." Acoust. Sci. & Tech. **24**(6): 382-385.
- 30 Nocke, C. (2000). In-situ Messung der akustischen (Wand-) Impedanz. Department of Physics. Oldenburg, Carl-von-Ossietzky Universität Oldenburg.
- 31 Taherzadeh, S. and K. Attenborough (1999). "Deduction of ground impedance from measurements of excess attenuation spectra." Journal of the Acoustical Society of America **105**(3): 2039-2042.
- 32 Hutchinson-Howorth, C., K. Attenborough, et al. (1993). "Indirect in situ and free-field measurement of impedance model parameters or surface impedance of porous layers." Applied Acoustics **39**: 77-117.
- 33 Allard, J. F., Y. Champoux, et al. (1989). "Pressure variation above a layer of absorbing material and impedance measurement at oblique incidence and low frequencies." Journal of the Acoustical Society of America **86**(2): 766-770.
- 34 Legouis, T. and J. Nicolas (1987). "Phase gradient method of measuring the acoustic impedance of materials." Journal of the Acoustical Society of America **81**(1): 44-50.
- 35 Daigle, G. A. and M. R. Stinson (1987). "Impedance of grass-covered ground at low frequencies measured using a phase difference technique." Journal of the Acoustical Society of America **81**(1): 62-68.
- 36 Zuckerwar, A. J. (1983). "Acoustic ground impedance meter." Journal of the Acoustical Society of America **73**(6): 2180-2186.
- 37 Attenborough, K. (1994). "A note on short-range ground characterisation." Journal of the Acoustical Society of America **95**(6): 3103-3108.
- 38 Allard, J.F. and Sieben, B. (1985). "Measurement of acoustic impedance in a free field with two microphones and a spectrum analyzer." Journal of the Acoustical Society of America **77**(4): 1617-1618.
- 39 Allard, J.F. and Champoux, Y. (1989). "In situ two-microphone technique for the measurement of the acoustic surface impedance of materials." Noise Control Eng. J. **32**(1): 15-23.
- 40 Allard, J.F. and Akine, A. (1985). "Acoustic impedance measurement with a sound intensity meter." Applied Acoustics **18**: 69-75.
- 41 Champoux, Y. and Nicolas, J. (1988). "Measurement of acoustic impedance in a free field at low frequencies." Journal of Sound and Vibration **125**(2): 313-323
- 42 Champoux, Y. and L'Espérance, A. (1988). "Numerical evaluation of errors associated with the measurement of acoustic impedance in a free field using two microphones and a spectrum analyzer." Journal of the Acoustical Society of America **84**(1): 30-38.
- 43 Li, J. F. and M. Hodgson (1997). "Use of pseudo-random sequences and a single microphone to measure surface impedance at oblique incidence." J. Acoust. Soc. Am. **104**(2): 2200-2210.
- 44 Alvarez, J. D. and F. Jacobsen (2007). In-situ measurements of the complex acoustic impedance of porous materials. Internoise, Istanbul.
- 45 Lanoye, R., H. E. de Bree, et al. (2004). A practical device to determine the reflection coefficient of acoustic materials in-situ based on a Microflown and microphone sensor. ISMA, Leuven.
- 46 Nosko, M., E. Tijs, et al. (2008). A study of influences of the in situ surface impedance measurement technique. DAGA, Dresden.
- 47 de Bree, H. E., E. Tijs, et al. (2007). An ultra miniature measurement tool to measure the reflection coefficient of acoustic damping materials in situ. SAE Noise and Vibration, St. Charles.
- 48 Nobile, M. A. (1985). "Acoustic propagation over an impedance plane." Journal of the Acoustical Society of America **78**(4): 1325-1336.
- 49 Rudnick, I. (1947). "The Propagation of an Acoustic Wave along a Boundary." Journal of the Acoustical Society of America **19**: 348-356.
- 50 Chen, C.F. and Soroka, W.W. (1975). "Sound propagation along an impedance plane." Journal of Sound and Vibration **43**(1): 9-20
- 51 Attenborough, K. (1984). "Near-grazing Sound Propagation Over Open, Flat Continuous Terrain." Bulletin Acoustics Australia **13**(1).
- 52 Abramowitz, M. and Stegun, I. (1965). "Handbook of Mathematical Functions with Formulas, Graphs, and Mathematical Tables." This book is copyright free and readily available on the internet.
- 53 Li, K. M., S. Taherzadeh, et al. (1997). "Sound propagation from a dipole source near an impedance plane." Journal of the Acoustical Society of America **101**(6): 3343-3352.
- 54 Attenborough, K. (1985). "Acoustic impedance models for outdoor ground surfaces." Journal of Sound and Vibration **99**(4): 521-544.
- 55 Li, K. M., T. Waters-Fuller, et al. (1998). "Sound propagation from a point source over extended-

- reaction ground." Journal of the Acoustical Society of America **104**(2): 679-685.
- 56 Attenborough, K. and S. Taherzadeh (1995). "Propagation from a point source over a rough finite impedance boundary." Journal of the Acoustical Society of America **98**(3): 1717-1722.
- 57 Chambers, J. P., J. M. Sabatier, et al. (1997). "Grazing incidence propagation over a soft rough surface." Journal of the Acoustical Society of America **102**(1): 55-59.
- 58 Clifford, S. F. and R. J. Lataitis (1983). "Turbulence effects on acoustic wave propagation over a smooth surface." Journal of the Acoustical Society of America **73**(5): 1545-1550.
- 59 Johnson, M. A., R. Raspet, et al. (1987). "A turbulence model for sound propagation from an elevated source above level ground." Journal of the Acoustical Society of America **81**(3): 638-646.
- 60 Song, B. H. and J. S. Bolten (2000). "A transfer-matrix approach for estimating the characteristic impedance and wave numbers of limp and rigid materials." Journal of the Acoustical Society of America **107**(3): 1131-1152.
- 61 Embleton, T. F. W., J. E. Piercy, et al. (1983). "Effective flow resistivity of ground surfaces determined by acoustical measurements." Journal of the Acoustical Society of America **74**(4): 1239-1244.
- 62 Hess, H., K. Attenborough, et al. (1990). "Ground characterization by short-range propagation." Journal of the Acoustical Society of America **87**(5): 1975-1986.
- 63 Attenborough, K. (1992). "Ground parameter information for propagation modeling." Journal of the Acoustical Society of America **92**(1): 418-427.
- 64 Biot, M. A. (1962). "Generalized Theory of Acoustic Propagation in Porous Media." J. Acoust. Soc. Am. **34**(9): 1254-1264.
- 65 Delany, M. E. and E. N. Bazley (1970). "Acoustical properties of fibrous absorbent materials." Applied Acoustics **3**: 105-116.
- 66 Miki Y. (1990). "Acoustical properties of porous materials - Modifications of Delany-Bazley models." J. Acoust. Soc. Jpn **11**(1): 19-24
- 67 Rayleigh J.W.S. (1877). "The theory of sound." Dover Publications
- 68 Attenborough, K. (1983). "Acoustical characteristics of rigid fibrous absorbents and granular materials." Journal of the Acoustical Society of America **73**(3): 785-799.
- 69 Hess, H., K. Attenborough, et al. (1990). "Ground characterization by short-range propagation." Journal of the Acoustical Society of America **87**(5): 1975-1986.
- 70 Sabatier, J. M., R. Raspet, et al. (1993). "An improved procedure for the determination of ground parameters using level difference measurements." Journal of the Acoustical Society of America **94**(1): 396-399.
- 71 Attenborough, K. (1988). "On the application of rigid-porous models to impedance data for snow." Journal of Sound and Vibration **124**(2): 315-327.
- 72 Sabatier, J. M., H. Hess, et al. (1990). "In situ measurements of soil physical properties by acoustical techniques." Journal of the Soil Science Society of America **54**: 658-672.
- 73 Martens, M. J. M., L. A. M. Vanderheijden, et al. (1985). "Classification of Soils Based on Acoustic-Impedance, Air-Flow Resistivity, and Other Physical Soil Parameters." Journal of the Acoustical Society of America **78**(3): 970-980.
- 74 Bérengier, M., M. R. Stinson, et al. (1997). "Porous road pavements: Acoustical characterization and propagation effects." Journal of the Acoustical Society of America **101**(1): 155-162.
- 75 Cramond, A. J. and C. G. Don (1987). "Effects of moisture content on soil impedance." Journal of the Acoustical Society of America **82**(1): 293-301.
- 76 Horoshenkov, K. V. and M. H. A. Mohamed (2006). "Experimental investigation of the effects of water saturation on the acoustic admittance of sandy soils." Journal of the Acoustical Society of America **120**(4): 1910-1921.
- 77 Chu WT. Single-microphone method for certain applications of the sound intensity technique. Journal of Sound and Vibration (1985); **101**(3): 443-445
- 78 Chung JY, Blaser DA. Transfer function method of measuring in-duct acoustic properties. I. Theory. Journal of the Acoustical Society of America (1980); **63**(3): 907-913
- 79 Ritter T. (2008). "Investigation on in-situ measurement of acoustic ground impedance outdoors." Institute of Physics. Oldenburg, Carl-von-Ossietzky Universität Oldenburg.



## XV. Table of abbreviations

2PA	Two parameter model	u	Particle velocity
ANSI	American National Standards Institute	$u_i$	.. in direction I
c	Speed of sound	V	Volume
$c_0$	.. in air	w	Faddeeva function
CEN	European Committee for Standardization	z	Height above surface
d	Distance	Z	Surface impedance, normalised
DB	Delany-Bazely (model)	$Z_c$	Characteristic impedance, normalised
EA	Excess attenuation	$Z_0$	.. of air, non-normalised
erf	Error function	$Z_e$	Effective surface impedance, normalised
erfc	Complementary ..	$Z_i$	Field impedance
f	Frequency	$Z_{MP}$	.. at midpoint, normalised
F	Boundary loss function	$\alpha$	Absorption coefficient
FT	Fourier transform	$\dot{\alpha}$	Rate of change of porosity
$H_{12}$	Transfer function	$\alpha_e$	Effective ..
H1A	One parameter model	$\beta$	Surface admittance
H3A	Three parameter model	$\beta_e$	Effective ..
H4A	Exact micro-structural model	$\gamma$	Ratio of specific heats in air
$h_{rl}$	Lower microphone height	$\delta$	Dirac function
$h_{ru}$	Upper microphone height	$\Delta$	Finite difference
$h_s$	Source height	$\theta$	Angle of incidence
I	$\sqrt{-1}$	$\lambda$	Wave length
Im	Imaginary part	$\lambda$	Numerical distance
ISO	International Organization for Standardization	$\nabla$	Gradient operator
$J_0$	Cylindrical Bessel function of zeroth order	$\rho_0$	Density of air
$J_1$	.. of first order	$\rho_m$	Density of material
k	Wave number in air	$\sigma$	Flow resistivity, static
$k_m$	Wave number, non-normalised	$\sigma_e, \sigma_{pe}$	Flow resistivity, effective
$k'$	Wave number, normalised	$\sigma_{eff}$	.., DB model
$L_0$	Scale of turbulence	$\sigma_v$	Mean roughness height
LD	Level difference	$\Phi$	Velocity potential
m	Ratio of complex densities	$\psi$	Phase of Q
Miki	Miki (improved DB) model	$\Omega$	Porosity
$n'$	Grain shape factor	$\omega$	Angular frequency
$N_{pr}$	Prandtl number		
p	Sound pressure		
Q	Spherical wave reflection coefficient		
$q^2$	Tortuosity		
R	Radial distance source-receiver		
$R_1$	Radial distance source-point of specular reflection		
$r_1$	Length of direct path		
$r_1'$	Length of reflected path		
Re	Real part		
$R_p$	Plane wave reflection coefficient		
$R_s$	Plane wave like reflection coefficient		
S	Surface area		
$s_f$	Shape factor ratio		
$s_p$	Pore shape factor		
t	Time		
$T_{60}$	Reverberation time		
TS	Technical specification		



## **Erklärung**

Hiermit versichere ich, dass ich die vorliegende Arbeit selbständig verfasst und keine anderen als die angegebenen Hilfsmittel und Quellen benutzt habe.

Oldenburg, den 26. Aug. 2008

# Lebenslauf

## Persönliche Daten

Name	Roland Kruse
Geburtsdatum	23.12.1975
Geburtsort	Oldenburg
Familienstand	ledig
Staatsangehörigkeit	deutsch
Anschrift	Karpfenweg 9 26127 Oldenburg

## Beruflicher Werdegang

April 2002 – heute :

Wissenschaftlicher Mitarbeiter am Institut für Physik / Arbeitsgruppe Akustik der Universität Oldenburg im Forschungsvorhaben  
FACE (Friendly Aircraft Cabin Environment, EU) und  
KOLOS (Kostengünstiger Lasersensor für optische Schwingungsmessung, BMWi)

Oktober 2002 – Dezember 2002 :

Lehrauftrag „Projektpraktikum Elektroakustik“ an der  
Fachhochschule Oldenburg/Ostfriesland/Wilhelmshaven,  
Studiengang Hörtechnik und Audiologie

## Bildungsgang

August 1983 – Juli 1986 :

Grundschule Nadorst, Eßkamp 6, Oldenburg

August 1986 – Juli 1988 :

Orientierungsstufe im Schulzentrum am Flötenteich, Hochheider Weg 169, Oldenburg

August 1988 – Juli 1992 :

Gymnasium im Schulzentrum am Flötenteich, Hochheider Weg 169,  
Oldenburg

August 1992 – Juli 1995 :

Technisches Gymnasium der Berufsbildenden Schulen II, Straßburger Str. 2,  
Oldenburg

Erwerb der allgemeinen Hochschulreife am 1.06.1995

Juli 1995 – Juni 1996 :

Wehrdienst

Oktober 1996 – März 2002 :

Studium der Marinen Umweltwissenschaften an der  
Carl von Ossietzky – Universität Oldenburg  
Erwerb des Diploms am 22.03.2002